

CHARGE-COUPLED DEVICE SPECTRA OF ASTEROIDS. I. NEAR-EARTH AND 3:1 RESONANCE ASTEROIDS^{a)}

JANE X. LUU^{b),c)}

Department of Earth, Atmospheric and Planetary Sciences, Massachusetts Institute of Technology, Massachusetts 02139

DAVID C. JEWITT^{b)}

Institute for Astronomy, University of Hawaii, 2680 Woodlawn Drive, Honolulu, Hawaii 96822

Received 2 August 1989; revised 8 March 1990

ABSTRACT

Main-belt asteroids and cometary nuclei are both frequently suggested sources of the relatively short-lived near-Earth asteroids (NEAs). We examine the asteroidal origin hypothesis by obtaining new high-quality charge-coupled device reflectivity spectra of 19 NEAs and 23 asteroids near the 3:1 resonance, and by performing a systematic comparison of these two groups of spectra. The comparison makes allowances for phase reddening in the colors of NEAs and for the differential albedo bias as discussed by Luu and Jewitt (1989a). We employ nonparametric statistical tests to check for consistency between the color distributions of the two populations. The tests indicate that the difference between the two distributions is generally not significant at the 3σ level; however, this conclusion is dependent on the (unknown) size distribution of the NEAs. Our observations are thus compatible with the hypothesis that the NEAs are derived from the 3:1 resonance region, but do *not* imply that this is the only possible source region. As a by-product of this survey, we detect solid-state absorption features in the spectra of three NEAs. These features have no counterparts in the spectra of the main-belt asteroids.

1. INTRODUCTION

a) Past Work

The near-Earth asteroids (NEAs) have gained prominence as an enigmatic group of asteroids occupying orbits that can bring them very close to Earth. Much of the interest in these bodies stems from the mystery surrounding their origin. Due to collisions and gravitational interactions with the Terrestrial planets, the NEAs have dynamical lifetimes ($\sim 10^7$ – 10^8 yr) which are short relative to the age of the solar system (e.g., Shoemaker *et al.* 1979). Moreover, the cratering rate in the inner solar system has been nearly constant over the last 3 billion years (Shoemaker and Wolfe 1986), hence we cannot assume that the present NEAs are the last remnants of a once much larger population. Instead, there must be a long-lived source elsewhere in the solar system in order to provide the observed flux of NEAs.

Frequently suggested sources have included both the main-belt asteroids and extinct comet nuclei. Mainbelt regions that are depleted in asteroids, such as the Kirkwood gaps at the 3:1 and 5:2 resonances, are plausible candidate source regions. On the other hand, many NEAs have exhibited what, up to now, have been regarded as exclusively cometary characteristics. For instance, a number of NEAs possess comet-like orbits (e.g., Hahn and Rickman 1985). Several NEAs (e.g., 2212 Hephaistos and 3200 Phaethon)

are dynamically associated with meteor streams, long considered to be debris ejected from comets (Drummond 1982; Whipple 1983; Olsson-Steel 1988). Furthermore, physical observations of other NEAs, such as 2101 Adonis (Ostro 1985) and 2201 Oljato (McFadden *et al.* 1984), have hinted at characteristics which are not normally associated with asteroids. Although none of these characteristics has yet been understood, there are enough tantalizing clues (plus a strong desire to identify the end fate of extinct comets) to force us to consider the comets as a possible source of the NEAs. At the current time, both the asteroidal and cometary origins appear to enjoy equal popularity in the astronomical community, and it appears likely that both sources contribute in some capacity to the NEA population. Wetherill (1988) has tentatively estimated that 60% of the NEA population is derived from the main belt, but the relative contributions of the two sources are not known with confidence.

Systematic studies of NEAs as a group are discouraged by their relatively short optimal window of visibility, their small sizes, and their large angular velocities. Despite these practical difficulties, various groups of observers have attempted to observationally address the issue of an asteroidal origin for the NEAs (McFadden *et al.* 1984; McFadden *et al.* 1985; Tedesco and Gradie 1987). McFadden *et al.* (1985) compared individual reflectances (from narrow-band photometry) of NEAs with the reflectances of selected planets, satellites, and specifically, asteroids near the 5:2 resonance (located at heliocentric distance $R = 2.8$ AU), in an effort to identify main-belt parent bodies for the NEAs. They established similarities between the spectral signatures of a few NEAs and 5:2 resonance asteroids, and came to the conclusion that a significant fraction of the NEA population could come from the 5:2 resonance region. Tedesco and Gradie (1987) attempted to classify the NEAs and compared their taxonomic distribution with the main-belt distribution at various resonances, including the 3:1 resonance (located

^{a)} Observations taken at the McGraw–Hill Observatory, Kitt Peak, which is operated by a three-university consortium consisting of University of Michigan, Dartmouth College, and M.I.T.

^{b)} Visiting Astronomer, Kitt Peak National Observatory, National Optical Astronomy Observatories, operated by the Association of Universities for Research in Astronomy, Inc., under contract with the National Science Foundation.

^{c)} Current address: Digital Siberia, Institute for Astronomy, 2680 Woodlawn Drive, Honolulu, HI 96822.

at $R = 2.50$ AU) and the 5:2 resonance. From their determination of the compositional distribution of the NEAs, they reached the conclusion that the resonances in the main belt are much more likely sources than comet nuclei. From this conclusion, they also suggested that extinct comet nuclei must be rare among NEAs, if they exist at all.

The main problem with the comparison of NEAs with the main-belt population stems from our poor knowledge of the true distribution of the compositions of the NEAs. It is known that the number of *S*- and *C*-type asteroids in the main belt is a function of heliocentric distance (Zellner 1979; Gradie and Tedesco 1982). At the 3:1 and 5:2 Kirkwood gaps, the number of *C* types is comparable to or greater than the number of *S* types. Among the NEAs, however, past observational data have indicated an excess number of *S* types with respect to the number of *C* types (Tholen 1984; Zellner *et al.* 1985; Veeder *et al.* 1989). The excess of *S* types (high albedo objects) has recently been shown to be consistent with an albedo bias (Luu and Jewitt 1989a, hereafter referred to as LJ89), but the problem was not adequately addressed in the NEA surveys by McFadden *et al.* (1985) or Tedesco and Gradie (1987), and the true distribution of the NEAs remains uncertain.

b) This Work

In this paper we attempt a systematic comparison of the optical reflectance spectra of a sample of NEAs with a sample of main-belt asteroids from near the 3:1 resonance. Of the resonances, the 3:1 resonance is among the most promising since it possesses a quantitatively demonstrated transport mechanism for bringing asteroids into the near-Earth region. Wisdom (1982) showed that asteroids near the 3:1 resonance can develop chaotic trajectories characterized by sudden jumps in eccentricity. These jumps in eccentricity are substantial enough to bring them into Mars-crossing orbits, and possibly Earth-crossing orbits as well. Once the asteroids are on Mars- or Earth-crossing trajectories, the probabilities of collisions with these planets appear sufficient to explain the depletion of asteroids in the Kirkwood gap at the 3:1 resonance (Wisdom 1983). As supporting evidence for this theory, the boundaries of the chaotic zone found by Wisdom agree well with the boundaries of the Kirkwood gap (Wisdom 1983). Given the validity of the transport mechanism for removing asteroids from the 3:1 resonance region, the question remains "do the physical properties of the NEAs support an asteroidal origin?"

This question motivates the present comparison, the objective of which is to check for consistency the hypothesis that the NEAs are derived from the 3:1 resonance in the main belt. By definition, the following test cannot *prove* that the NEAs are derived from the 3:1 resonance, or for that matter, from any particular source location. We intend only to determine whether the favored 3:1 resonance is a plausible source region for the NEAs, as judged by observational data. Our comparison parameter will be the optical reflectivity gradients of the asteroids, i.e., the colors of the asteroids in the optical.

The optical colors of the NEAs and the 3:1 resonance asteroids will be compared using two standard nonparametric statistical tests, the Mann-Whitney U test (Conover 1980; Mendenhall *et al.* 1986) and the Kolmogorov-Smirnov test (Gibbons 1985; Dickinson 1985).

In summary, four aspects of the present survey distinguish it from previous surveys.

(1) Unlike previous studies, we use a completely homogeneous data set. Our observations of the NEAs and of the 3:1 resonance asteroids are taken using identical instrumentation on the same nights, and the resulting spectra are reduced and interpreted according to uniform procedures.

(2) We correct for the albedo bias. The albedo bias favors observations of large, bright objects over small, dark ones, and causes an overrepresentation of bright asteroids in optical surveys. Treatment of the albedo bias is crucial in the context of the present study, since the bias is different for the NEAs and for the main-belt asteroids. LJ89 used a Monte Carlo model to calculate the albedo bias in optical observations of NEAs and showed that this albedo bias can account for the apparent *S*-type excess among the NEAs. We will use the LJ89 model to account for the bias in our analysis. Albedo bias was either not addressed, or addressed in an incomplete way, in previous studies.

(3) We consider phase reddening in our analysis. Phase reddening selectively reddens the NEAs, since these are typically observed at much larger phase angles than are the main-belt asteroids. Typical color-phase coefficients are small (0.001–0.002 mag/degree), but it is clear that the apparent color index of an asteroid observed at phase angle $\alpha = 100^\circ$ could easily be in error by 0.1–0.2 mag if the color-phase bias were to be neglected. Previous studies did not incorporate the color-phase bias.

(4) Our study is based on spectra taken with a charge-coupled device (CCD) spectrograph, whereas previous studies of the colors of asteroids have generally used multifilter photometric measurements taken with photomultiplier tubes. Detector technology has now advanced to the point where measurements of comparable signal-to-noise and much greater spectral resolution can be taken with a CCD spectrograph in a comparable or shorter amount of observing time. The main advantages conveyed by the CCD spectrographs are (1) higher spectral resolution, (2) high quantum efficiency at a wide range of wavelengths, thus allowing us to sample fainter objects, and (3) spatial resolution along the spectrograph slit which allows accurate, *simultaneous* sky background subtraction. Narrow absorption and emission features, which may be missed by filters, would be apparent even at moderate dispersion in a CCD spectrum. Indeed, two asteroids from our current data show weak absorption features previously undetectable with conventional narrowband photometry (see Sec. III). At 5 Å/pixel, an average-sized CCD chip (500 × 500 pixels) can cover a wavelength range of 2500 Å in one exposure. One single exposure yields a continuous spectrum that can only be acquired in a narrowband-filter observing program with many exposures and many filter changes. This efficiency, coupled with the linearity and high sensitivity of CCDs, makes the CCD spectrograph the ideal instrument for moderate to high-resolution spectroscopy of faint objects.

II. OBSERVATIONS

a) Instrumentation

The present spectra were taken with the "Mk III" spectrograph at the McGraw-Hill Observatory (MHO) 2.4 m telescope in August and September 1988, and with the "Gold-Cam" spectrograph at the Kitt Peak National Observatory (KPNO) 2.1 m telescope in October 1988 and February 1989. The Mk III was attached to the $f/7.5$ Cassegrain focus of the MHO 2.4 m. The detector used in the spectrograph

was a Thomson CCD (400×576 pixels) with a readout noise of ± 7 electrons. All MHO spectra described in this paper were taken with a 300 line/mm grating blazed at wavelength $\lambda = 5000 \text{ \AA}$ and used in the first order. The projected dimensions of the slit were $2.8'' \times 320''$, and the slit was oriented North-South. The Thomson CCD has $22 \mu\text{m}$ square pixels, yielding a dispersion of 5.1 \AA/pixel in the wavelength direction and a scale of $0.73''/\text{pixel}$ in the spatial direction. Spectral coverage was limited to $4200 \leq \lambda \leq 7200 \text{ \AA}$ to fully exploit the sensitivity of the instrument. The relatively wide ($2.8''$) slit limits the effective resolution to 20 \AA full width at half maximum (FWHM). We chose a wide slit in anticipation of dealing with two specific problems: (1) the NEAs are often faint, fast moving objects. A wide slit minimizes the risk of signal loss due to telescope guiding errors; (2) when taking spectra at nonzero zenith angles, one must deal with differential refraction, which can easily distort the true spectrum obtained with a narrow slit (Filippenko 1982).

At the $f/7.7$ Cassegrain focus of the KPNO 2.1 m telescope, the GoldCam spectrograph was configured to simulate the Mk III as closely as possible (within the confines of the GoldCam design). The GoldCam spectrograph contained an 800×800 TI CCD, with a readout noise of ± 9 electrons. The projected dimensions of the slit were $2.8'' \times 150''$, and the slit was oriented in the East-West direction in October 1988 and North-South in February 1989. The spatial resolution of the spectrograph was $0.79''/\text{pixel}$. A 150 lines/mm grating used in first order and blazed at $\lambda = 5000 \text{ \AA}$ yielded a dispersion of 4.9 \AA/pixel . The spectral range coverage was $3600 \leq \lambda \leq 7400 \text{ \AA}$, and the effective resolution was once again $\sim 20 \text{ \AA}$ FWHM. A summary of the instrument configurations is presented in Table I.

The integration times were varied according to the brightness of each object. The object was located in the center of the slit using a down-looking TV camera to examine a reflection from the slit jaws. The telescope was typically tracked at the rates of the object, although guiding at sidereal rate was sometimes used if the object was moving very slowly. We monitored the accuracy of the telescope tracking with the down-looking guider TV system and estimated the guiding errors to be substantially smaller than the slit width. Objects fainter than $m_V \sim 18.5$ could not be seen in the reflection from the spectrograph slit and had to be guided "blind." In these cases, the telescope was tracked at the rate of the object

and the integrations were periodically paused to verify the centering of the asteroid in a (more sensitive) up-looking finder TV. At least two independent integrations were taken on each object in order to combine the spectra later on for a higher quality spectrum. The comparison of the signal in the repeated spectra demonstrates the repeatability of the pointing and the guiding.

For wavelength and flux calibration purposes, spectra of helium-neon-argon lamps and standard stars were recorded at frequent intervals throughout each night. The stars were selected from the catalogs of IIDS (Oke 1974) and IRS (Stone 1977) standards. Observations of the standard stars were coordinated so that the stars were observed at airmasses similar to those of the asteroids (the airmass difference was ≤ 0.1 in each case). In anticipation of the need to calculate the reflectivity gradients from the asteroid spectra, we also observed solar-type stars each night. In August and October 1988, the solar-type star 16 Cyg B was used as the solar analog for the 1988 data reduction (Hardorp 1978, 1980). In February 1989, 16 Cyg B was not visible, hence the solar-type star Hyades 64 was used as the solar analog (Hardorp 1978, 1980). The spectra of the two solar analogs are compared below. At the MHO 2.4 m, flat fields were taken with a tungsten lamp, while a quartz lamp was used at the KPNO 2.1 m. A large number of flat fields (~ 100) were obtained each night and averaged to obtain a high signal-to-noise ratio.

b) Observed Asteroids

We obtained high-quality spectra of 19 NEAs and 23 asteroids near the 3:1 resonance in the time period August-October 1988 and February 1989. We define an asteroid as being near the 3:1 resonance if its semimajor axis a falls within the range $2.46 < a < 2.54 \text{ AU}$. This range is coincident with the semimajor axis range for the test asteroids used by Wisdom (1982, 1983) in his tests for chaotic trajectories in the 3:1 resonance region. A plot of eccentricity versus semimajor axis for all numbered resonance asteroids (as defined by the semimajor axis range described above) is presented in Fig. 1. The 23 observed resonance asteroids constitute 28% of this population (as of 1988). Of the entire sample of observed asteroids, 11 resonance asteroids and four NEAs were observed on more than one night, providing a good check on the repeatability of our spectra. A log of our obser-

TABLE I. Instrument log.

Telescope	$f/$ Ratio	Instrument	CCD Size	$\Delta\lambda$ FWHM	λ Range	Read Noise	Spatial Scale	Slit Size	Dispersion
2.4 m	7.5	Mk III	400 x 576	20 \AA	4200 - 7200 \AA	7 e ⁻	0.73'' / pixel	2.8'' x 320''	5.1 \AA / pixel
2.1 m	7.7	GoldCam	800 x 800	20 \AA	3600 - 7200 \AA	9 e ⁻	0.79'' / pixel	2.8'' x 150''	4.9 \AA / pixel

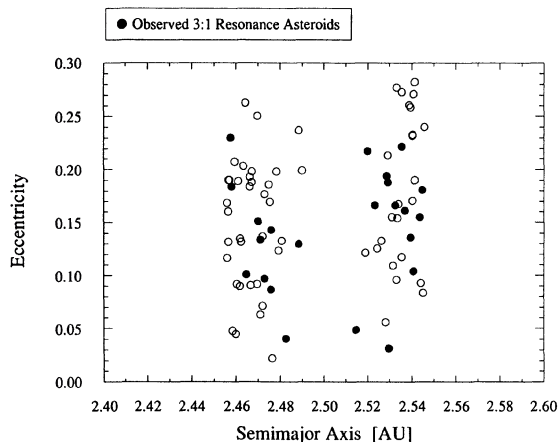


FIG. 1. Plot of eccentricity vs semimajor axis for all numbered asteroids near the 3:1 resonance (compiled from *Ephemerides of Minor Planets, 1988*). The filled circles are the resonance asteroids observed in our program.

variations appears in Tables II and III.

The apparent magnitudes of the observed asteroids fell in the range $m_V = 13$ –19. Although the NEAs are known to be smaller, on the average, than the known members of the main belt, the sensitivity of the CCD allowed us to observe unusually faint (small) main-belt asteroids, thus reducing the difference between the mean magnitudes of the two asteroid groups. A histogram of the absolute magnitudes of the observed asteroids (adopted from *Ephemerides of Minor Planets, 1988*) is shown in Fig. 2. The mean NEA absolute magnitude is $m_V(1,1,0) \approx 15.9$ while the mean resonance asteroid absolute magnitude is $m_V(1,1,0) \approx 12.1$. The difference is ~ 3.8 mag, corresponding to a factor of 5.8 in radius—a relatively small difference in size. Figure 2 illustrates the fact that the use of CCDs allowed us to observe smaller members of the main-belt population, thus reducing the size gap between the NEAs and the main-belt asteroids.

III. DATA REDUCTION

Most of the data reduction was performed using the software package IRAF running on a VAX 11-780 at the Institute for Astronomy. The steps of the data reduction procedure are summarized below.

(1) *Bias subtraction and cosmic ray removal.* The bias was subtracted from all spectra. Deviant pixels caused by cosmic rays were identified and removed from each spectrum by averaging over the neighboring pixels. The Thomson chip in the MK III spectrograph was more susceptible to cosmic rays than the TI chip in the GoldCam, but cosmic rays were well removed from both chips by IRAF.

(2) *“Flattening” the data.* Special care was taken to remove large scale structures (due to the color of the lamps) from the flat fields. To correct for vignetting from uneven illumination of the slit by the lamps, the slit profile was determined for each night. The slit profile and the flat field (with large scale structure removed) were combined to produce a new “flat” field, which then was divided into all spectra.

(3) *Background subtraction and collapsing the two-dimensional spectra.* After the spectra were flattened, the sky

background in each object spectrum was fitted individually for each wavelength and subtracted. It was seen that the most prominent night sky lines ($[O\ I]$ at $\lambda = 5577\ \text{\AA}$, $[O\ I]$ at $\lambda = 6300\ \text{\AA}$, and the $O_2\ B$ band at $\lambda = 6870\ \text{\AA}$) were well removed in most spectra, with the exceptions being mostly the spectra with a lower signal-to-noise ratio. The imperfectly subtracted sky lines leave behind spurious “features” which should be disregarded. No image distortion was visible in spectra from either spectrograph. As all the observed objects were point sources, the two-dimensional spectra were subsequently collapsed to one-dimension.

(4) *Wavelength calibration.* The dispersion solution for each He-Ne-Ar spectrum was determined individually in case the dispersion parameters changed during the night with the flexure of the spectrograph. The typical wavelength residuals in the linearized spectra were $\sim \pm 3\ \text{\AA}$, about 1/6th of the FWHM, and no significant time-dependent dispersion variations were found. Each object spectrum was then wavelength calibrated using the dispersion solution with the most comparable air mass.

(5) *Flux calibration and atmospheric extinction correction.* From the known flux densities of the standard stars, a sensitivity function for the instrument was computed for each night and applied to each asteroid spectrum. Errors due to extinction were minimized since the stars were observed at air masses similar to those of asteroids (airmass difference < 0.1). The errors in the standard star fluxes at a given wavelength and at widely different airmasses were generally $\leq 5\%$ across our wavelength range, confirming the insignificant amount of differential refraction. Similarly, the errors in asteroidal fluxes across the wavelength range were also limited to $\leq 5\%$. We attribute most of the flux calibration error to centering errors and small slit losses from variable seeing. With both the MK III and the GoldCam spectrographs, the asteroid spectra are noisy at the extreme blue end due to poor sensitivity in this spectral range. For this reason, the effective portion of the asteroid spectra used in this analysis includes only the range $4800 \leq \lambda \leq 7200\ \text{\AA}$.

(6) *Computing reflectivity (reflectance) spectra.* We used the solar analog 16 Cyg B to compute reflectivities from the flux calibrated asteroid spectra from 1988 (38 asteroids), and the solar analog Hyades 64 for the spectra from 1989 (4 asteroids). Division by the solar spectrum removed the solar lines from the asteroid reflectivities, although prominent solar absorption lines (e.g., $H\ I$ at $\lambda = 6563\ \text{\AA}$) were occasionally imperfectly divided, resulting in false “features.” An example of the repeatability of our spectra is illustrated in Fig. 3(a), where we show the unsmoothed ratio of two spectra of the solar analogue Hyades 64, taken on different nights (1989 February 3 and 1989 February 8). The ratio is normalized at $6000\ \text{\AA}$. It is seen that the ratio is essentially constant, with $\leq 1\%$ systematic deviation from the horizontal over the wavelength range used in the analysis ($4800 \leq \lambda \leq 7200\ \text{\AA}$). We also considered the possibility of systematic errors introduced by the use of two different solar analogues (16 Cyg B and Hyades 64). In Fig. 3(b), we show the unsmoothed spectrum of 16 Cyg B divided by Hyades 64 and normalized at $6000\ \text{\AA}$. The ratio shows only a slight slope, of order $1\%/10^3\ \text{\AA}$. The compatibility of the two solar analogues, plus the repeatability of the solar spectrum and of other repeated spectra places an upper limit ($\leq 1\%/10^3\ \text{\AA}$) on systematic reflectivity gradient errors that may arise due to division by different solar analogs.

The unsmoothed reflectivity spectra of the NEAs are

TABLE II. Journal of near-Earth asteroid observations.

Asteroid	UT Date [Yr Mo Day]	Instrument	$m_V(1,1,0)$	Semimajor Axis [AU]	R [AU]	Δ [AU]	Phase Angle [°]	m_V^1
1980	1988 08 08	Mk III	14.07	1.71	1.30	0.68	50.5	15.5
2100	1988 08 08	Mk III	16.12	0.83	1.18	0.78	58.1	18.0
2212	1988 10 06	GoldCam	14.00	2.16	2.97	2.08	10.5	18.5
3040	1989 02 03	GoldCam	14.70	1.84	1.68	0.74	16.6	16.0
3199	1988 08 05	Mk III	15.03	1.57	1.28	0.46	45.5	15.5
	1988 10 08	GoldCam	15.03	1.57	1.13	0.43	61.3	15.4
	1988 10 09	GoldCam	15.03	1.57	1.13	0.44	61.4	15.5
3200	1988 10 06	GoldCam	14.65	1.27	2.38	1.74	21.8	18.7
3271	1988 08 08	Mk III	16.90	2.10	1.31	0.62	48.8	18.1
3288	1988 08 07	Mk III	15.34	2.03	2.05	1.09	11.8	17.7
3362	1988 08 07	Mk III	18.0	0.99	1.13	0.48	63.4	18.7
3553	1988 10 08	GoldCam	16.8	1.64	1.87	1.03	22.1	19.2
3691	1989 02 03	GoldCam	14.90	1.77	1.58	0.65	18.2	15.8
	1989 02 08	GoldCam	14.90	1.77	1.56	0.61	16.0	15.6
3752	1988 08 08	Mk III	15.6	1.41	1.84	1.31	32.3	18.7
3838	1988 10 08	GoldCam	15.5	1.50	1.32	0.81	48.6	17.3
	1988 10 09	GoldCam	15.5	1.50	1.34	0.80	48.0	17.3
3908 (1980 PA)	1988 08 07	Mk III	17.7	1.93	1.31	0.30	13.1	16.3
	1988 10 06	GoldCam	17.7	1.93	1.05	0.06	34.2	13.1
	1988 10 10	GoldCam	17.7	1.92	1.05	0.06	37.3	13.1
1987 MB	1988 10 07	GoldCam	14.5	1.98	3.19	2.24	07.2	19.2
1985 DO2 (1988 OG)	1988 09 09	Mk III	15.0	1.82	1.27	0.28	14.1	13.4
1988 TA	1988 10 08	GoldCam	21.0	1.53	1.07	0.07	08.8	15.8
1988 VN4	1989 02 04	GoldCam	17.0	1.81	1.24	0.65	52.6	18.4
1989 AC	1989 02 04	GoldCam	14.5	2.60	1.35	0.43	27.6	14.5

¹ Estimated from $m_V(1,1,0)$.

TABLE III. Journal of 3:1 resonance asteroid observations.

Asteroid	UT Date [Yr Mo Day]	Instrument	m_V (1,1,0)	Semimajor Axis [AU]	R	Δ [AU]	Phase Angle [°]	m_V ¹	Asteroid	UT Date [Yr Mo Day]	Instrument	m_V (1,1,0)	Semimajor Axis [AU]	R	Δ [AU]	Phase Angle [°]	m_V ¹
198	1988 10 06	GoldCam	8.54	2.46	2.22	1.96	26.7	12.7	2599	1988 09 08	Mk III	12.27	2.54	2.13	1.13	02.9	14.5
292	1988 09 08	Mk III	10.28	2.53	2.48	1.82	20.6	14.6		1988 10 09	GoldCam	12.27	2.54	2.15	1.23	14.0	15.2
	1988 10 06	GoldCam	10.28	2.53	2.49	1.58	11.9	14.0	2832	1988 09 08	Mk III	12.50	2.47	2.69	1.74	9.3	16.4
495	1988 09 08	Mk III	10.97	2.49	2.23	1.23	3.7	13.5	2834	1988 09 09	Mk III	12.00	2.54	2.76	1.78	06.3	15.9
	1988 10 10	GoldCam	10.97	2.49	2.20	1.28	13.0	13.9	2927	1988 09 08	Mk III	12.23	2.53	2.33	2.30	25.1	17.0
518	1988 09 09	Mk III	11.44	2.54	2.29	1.83	25.2	15.7	2973	1988 09 08	Mk III	12.53	2.47	2.42	1.44	07.5	15.7
	1988 10 07	GoldCam	11.44	2.54	2.36	1.59	19.0	15.3	2984	1988 09 09	Mk III	13.16	2.47	2.71	1.70	01.9	16.7
556	1988 09 08	Mk III	9.32	2.46	2.65	1.77	13.2	13.4		1988 10 07	GoldCam	11.50	2.54	2.76	2.19	19.2	16.3
	1988 09 09	Mk III	9.32	2.46	2.65	1.78	13.5	13.4	3167	1988 10 08	GoldCam	11.50	2.54	2.76	2.18	19.1	16.2
650	1988 09 09	Mk III	13.03	2.46	2.01	1.52	29.3	16.7		1988 09 09	Mk III	13.60	2.52	2.26	1.26	03.2	16.1
1076	1988 09 09	Mk III	12.51	2.47	2.52	1.52	03.3	15.6	3218								
1722	1988 10 06	GoldCam	12.53	2.51	2.44	1.59	15.4	16.3									
1854	1988 09 08	Mk III	12.89	2.54	2.51	1.64	14.4	16.8									
	1988 10 06	GoldCam	12.89	2.54	2.47	1.47	02.5	16.0									
2113	1988 10 09	GoldCam	13.23	2.47	2.31	1.79	24.2	17.3									
2159	1988 09 08	Mk III	12.16	2.48	2.46	1.98	23.1	16.6									
	1988 10 06	GoldCam	12.16	2.48	2.45	.66	17.7	16.0									
2167	1988 09 08	GoldCam	11.70	2.54	2.97	2.03	08.7	16.1									
	1988 10 08	GoldCam	11.70	2.54	2.99	2.33	16.4	16.7									
2317	1988 09 08	Mk III	13.46	2.52	2.17	1.18	07.1	16.0									
	1988 10 10	GoldCam	13.46	2.52	2.14	1.18	10.5	16.1									
2339	1988 09 08	Mk III	13.55	2.53	2.04	1.03	02.2	15.4									
	1988 10 09	GoldCam	13.55	2.53	2.04	1.14	16.9	16.3									
2351	1988 09 09	Mk III	13.10	2.53	2.14	1.14	3.9	15.4									

¹ Estimated from m_V (1,1,0).

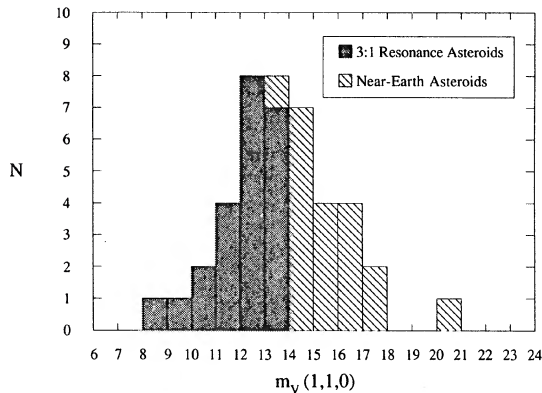


FIG. 2. Absolute magnitude $m_V(1,1,0)$ histogram for observed NEAs and asteroids near the 3:1 resonance.

shown in Fig. 4, while the unsmoothed spectra of the resonance asteroids are shown in Fig. 5. Most reflectivity spectra are of high quality, with a signal-to-noise of 20–100 per pixel for the resonance asteroid spectra shown in Fig. 5. The NEAs were typically fainter than the resonance asteroids

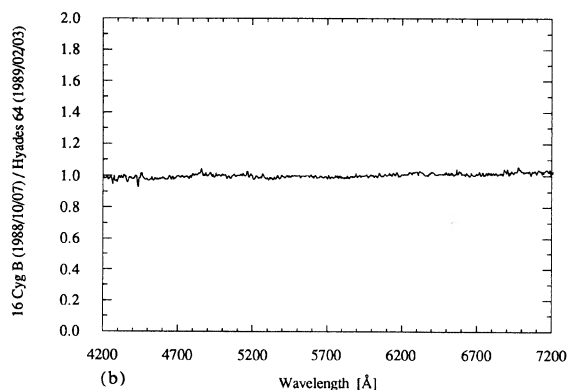
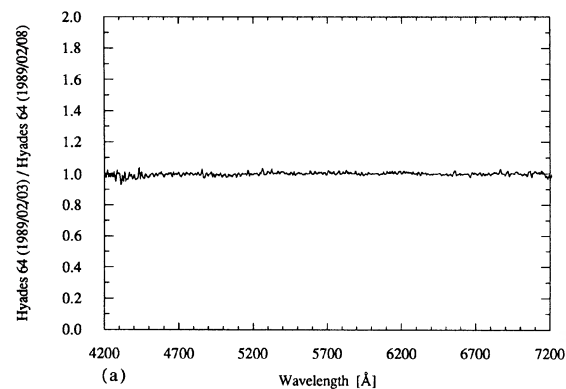


FIG. 3. (a) Normalized ratio of two spectra of the solar analog Hyades 64 taken on different nights (1989 February 3 and 1989 February 8), and (b) normalized ratio of 16 Cyg B divided by Hyades 64. Both ratios were normalized at 6000 Å.

(the faintest observed asteroids were NEAs), and their signal-to-noise lies in the range 4–100 per pixel (for example, see spectra of NEAs 1988 VN4 and 1980 PA in Fig. 4). The reflectivity spectra are typically smooth in shape, with the majority possessing a positive slope, indicating a red color with respect to the Sun. Except for the NEAs 3691, 1980 PA, and 1985 DO2, the spectra appear featureless at 20 Å resolution. In the spectra of 1980 PA and 1985 DO2 (Fig. 4), the features at 5050 and 5500 Å are real, as is the feature at 4800 Å in NEA 3691. The spectrum of 1980 PA extends further in the blue region than that of 1985 DO2, thus allowing also the detection of a feature at 4300 Å. We verified the existence of these features by repeating the observation of each of the three NEAs on different nights; the features were detected in every repeat observation. The features will be discussed in more detail in Sec. VIIIb.

IV. NORMALIZED REFLECTIVITY GRADIENT

Although the reflectivities of the asteroids in Figs. 4 and 5 are not perfectly linear functions of wavelength, the reflectivities of most are fitted very well with a straight line, providing an easily accessible, first-order quantitative parameter with which to compare the spectra of the asteroids. We therefore performed linear least-squares fits to the slope of each asteroid's reflectivity, in order to measure the reflectivity gradient $dS/d\lambda$, a measure of the color of the asteroid. The normalized reflectivity gradient S' (which we will also refer to as “color”) between wavelengths λ_1 and λ_2 is defined here as

$$S'(\lambda_1, \lambda_2) = \left(\frac{dS/d\lambda}{S_{6000}} \right), \quad (1)$$

where $dS/d\lambda$ is the rate of change of the reflectivity with respect to wavelength in the range $\lambda_1 \leq \lambda \leq \lambda_2$, and S_{6000} is the reflectivity at $\lambda = 6000$ Å. We normalize the reflectivity gradient at $\lambda = 6000$ Å because it lies near the center of our effective wavelength range. The apparent (uncorrected for phase) S' of each observed asteroid appears in Tables IV and V, where it is expressed in percent per 10^3 Å. Our wavelength range roughly spans the “V” filter and “R” filter bandpasses, making S' a spectroscopic analog of the $m_V - m_R$ color index. The approximate relation between our S' and $m_V - m_R$ is

$$m_V - m_R = 2.5 \log \left(\frac{2 + S' \Delta\lambda}{2 - S' \Delta\lambda} \right), \quad (2)$$

where S' is in $\%/10^3$ Å, $\Delta\lambda = \lambda_2 - \lambda_1$ is the difference in the effective wavelength (in 10^3 Å), and $m_V - m_R$ is the object color index minus the solar color index (in mag). Since we observed several asteroids on more than one night, a comparison of S' taken on different nights provides an empirical estimate of the errors of our reflectivity determinations. After correcting for the phase-reddening effect (see Sec. Va), we found that most of our values of S' were reproducible to $\Delta S' \sim 1\% - 2\%/10^3$ Å (corresponding to a color error 0.01–0.02 mag in $m_V - m_R$), regardless of the spectrograph used. The repeatability of S' indicates that extinction and differential refraction were not significant sources of error in our spectra. It is possible that some of the residual color “errors” at the $1\% - 2\%/10^3$ Å level reflect real rotational color variations on the asteroids, although we have no immediate test of this possibility.

The histograms of apparent S' for both populations were computed and are shown in Figs. 6(a) and 6(b). The NEA

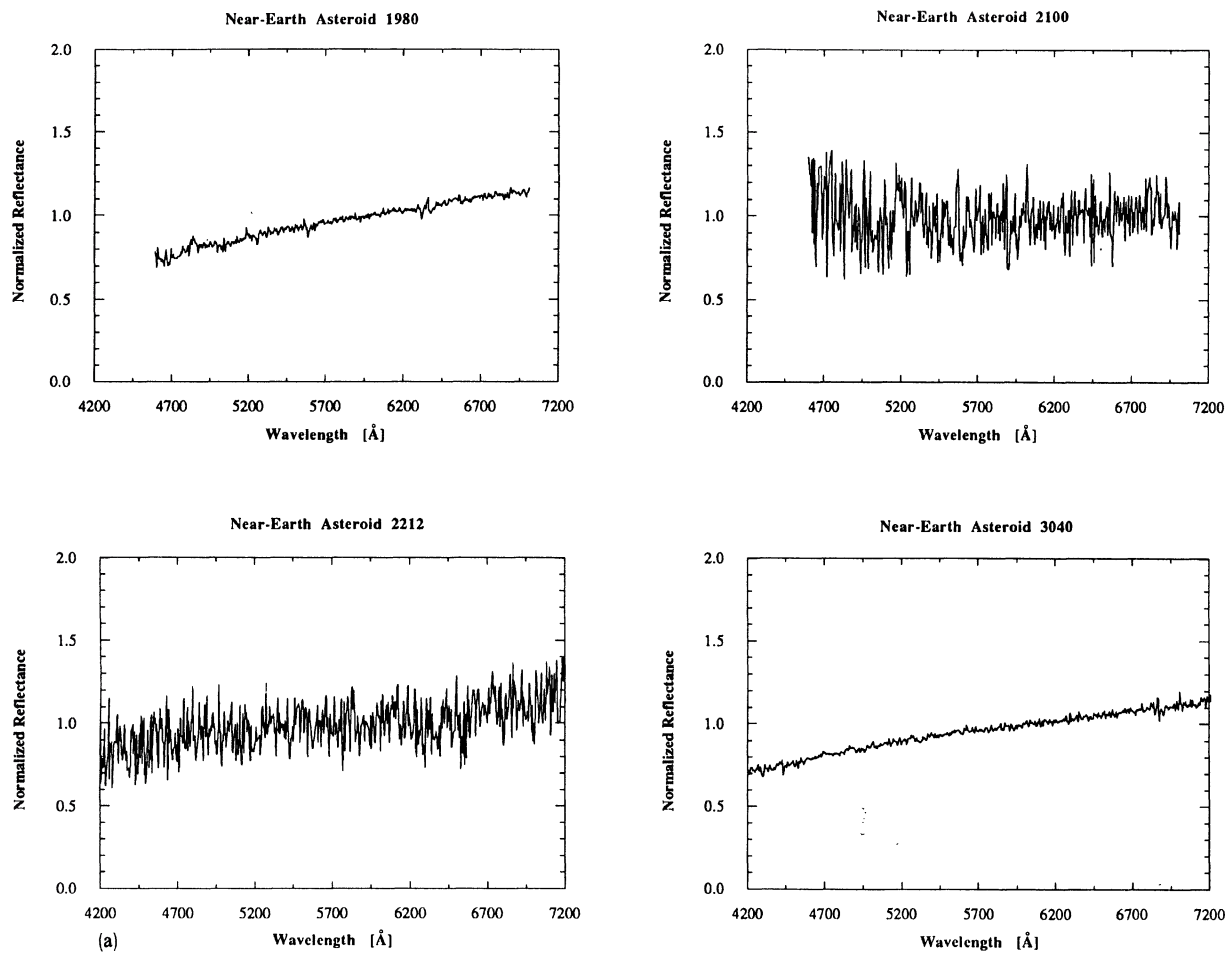


FIG. 4. Normalized reflectivity spectra of NEAs. Features at $\lambda = 5577 \text{ \AA}$, $\lambda = 6300 \text{ \AA}$, $\lambda = 6563 \text{ \AA}$, and $\lambda = 6870 \text{ \AA}$ are due to imperfect removal of sky and solar lines and are not intrinsic to the asteroids. Intrinsic absorption features in spectra of NEAs 3691, 1980 PA and 1985 DO2 are marked by arrows.

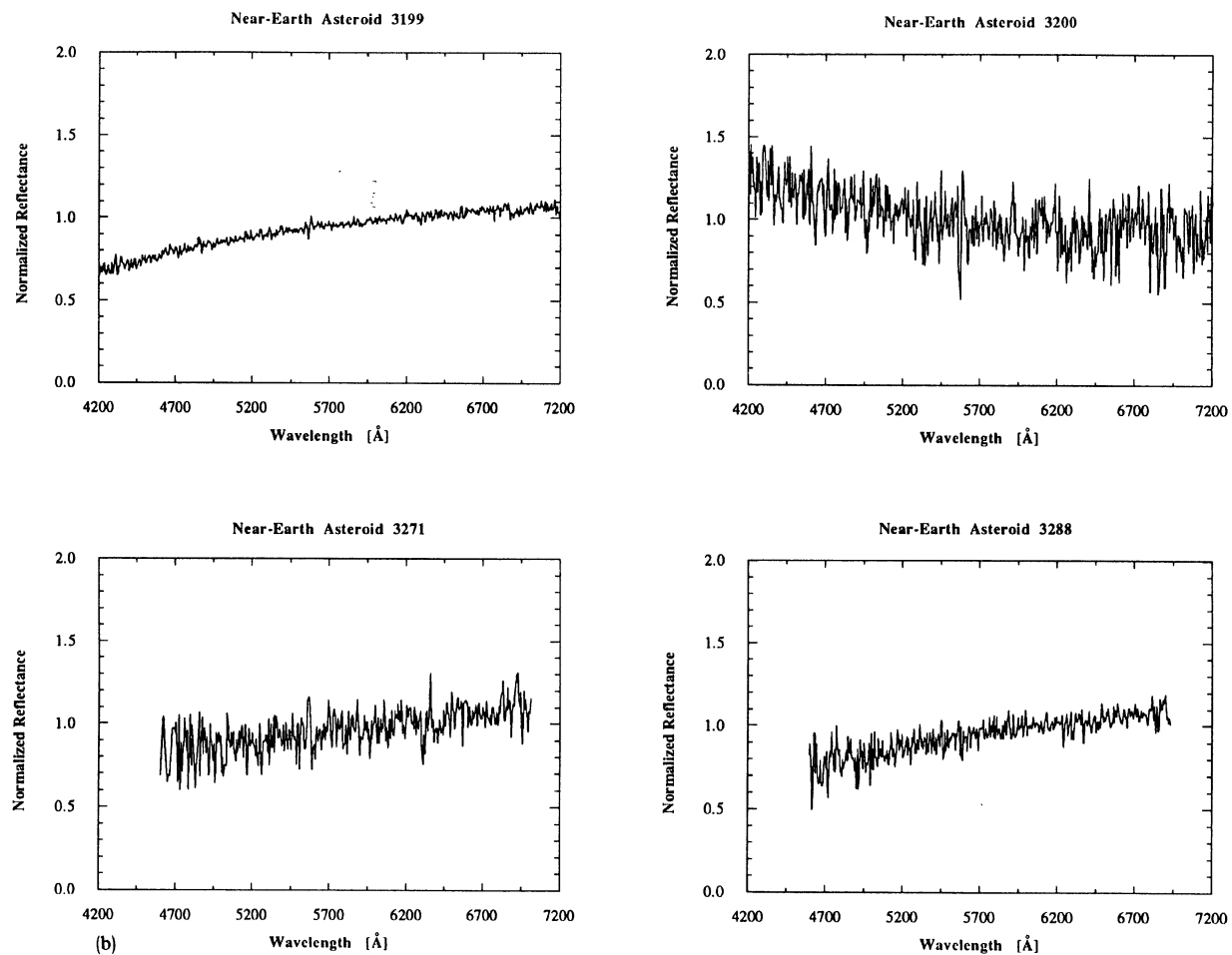


FIG. 4. (continued)

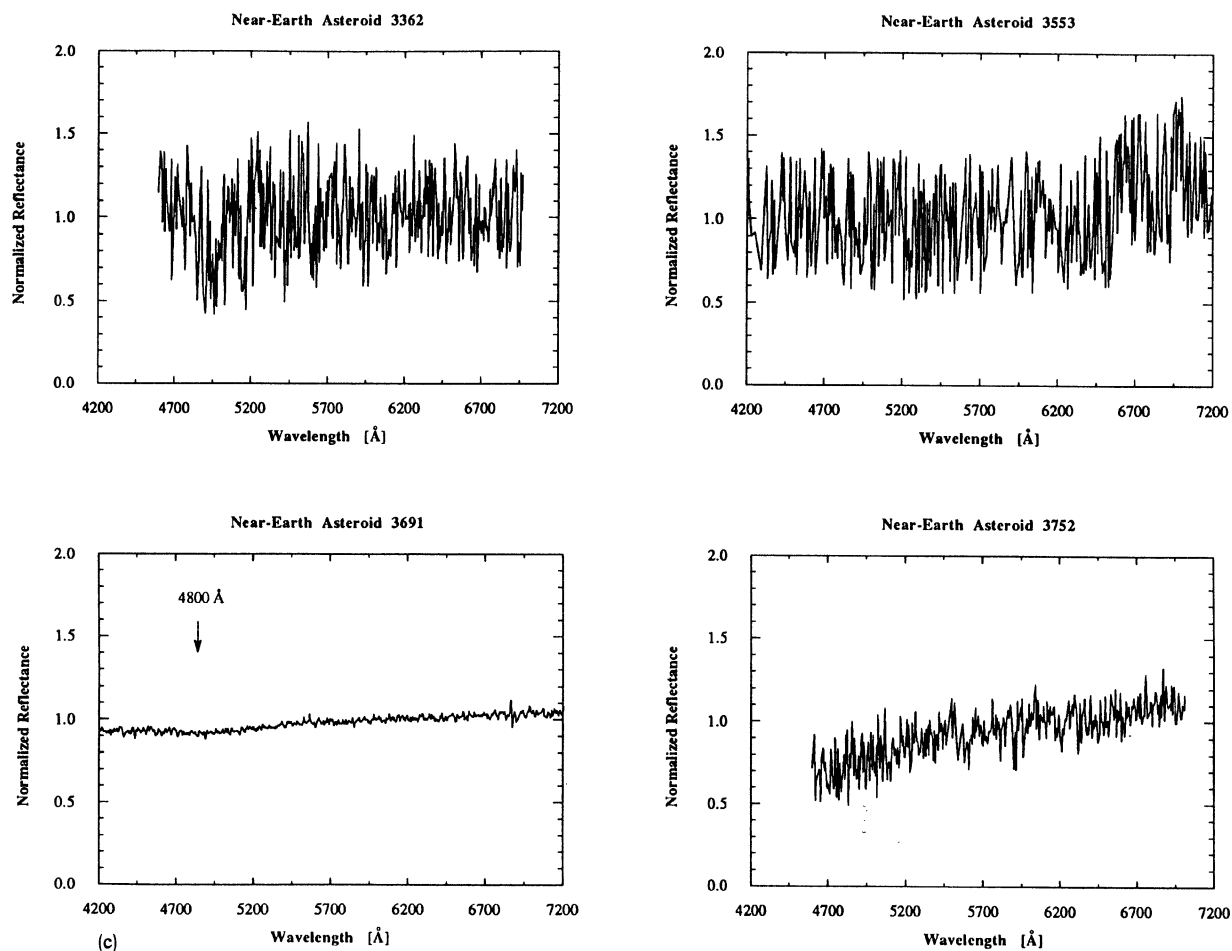


FIG. 4. (continued)

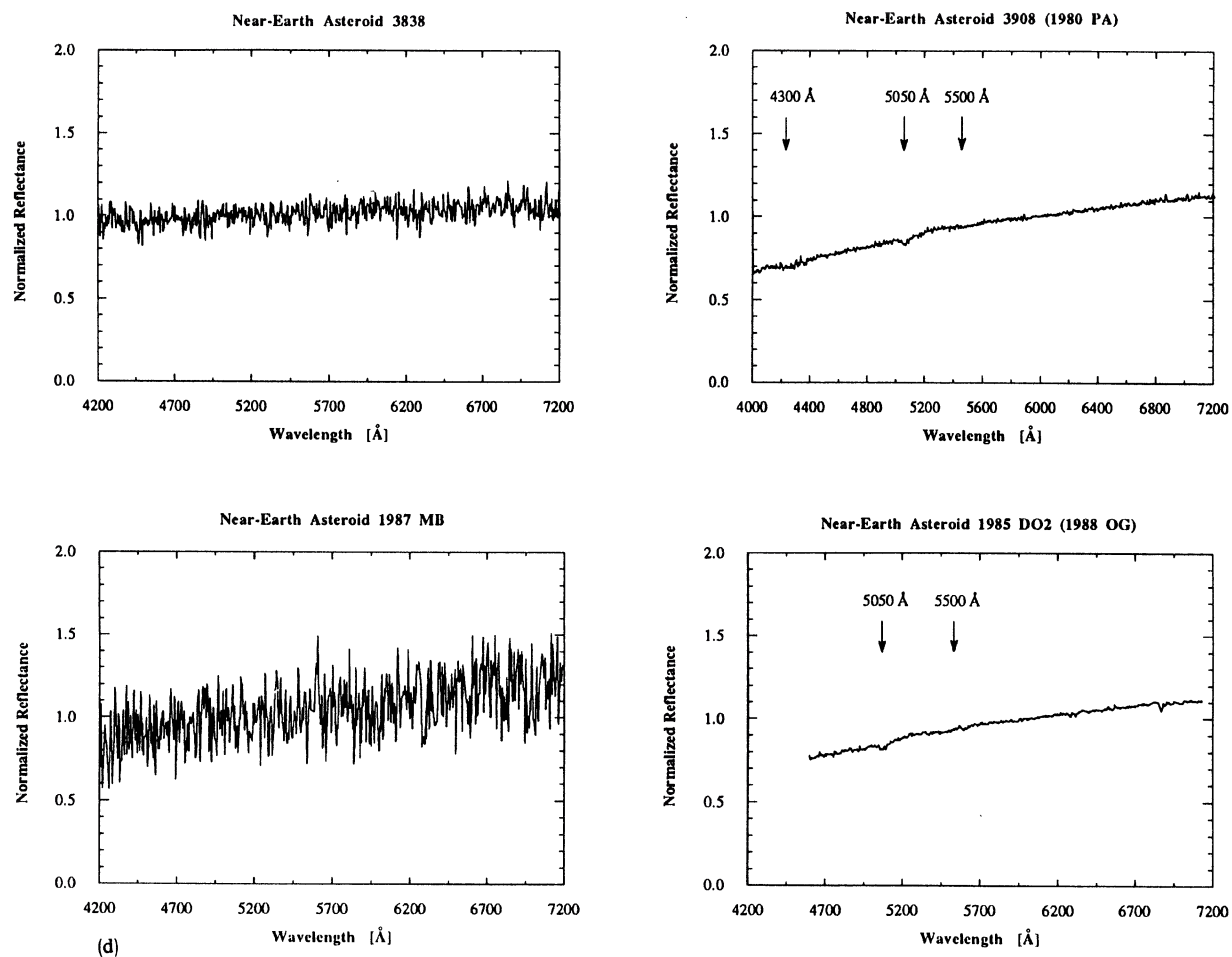


FIG. 4. (continued)

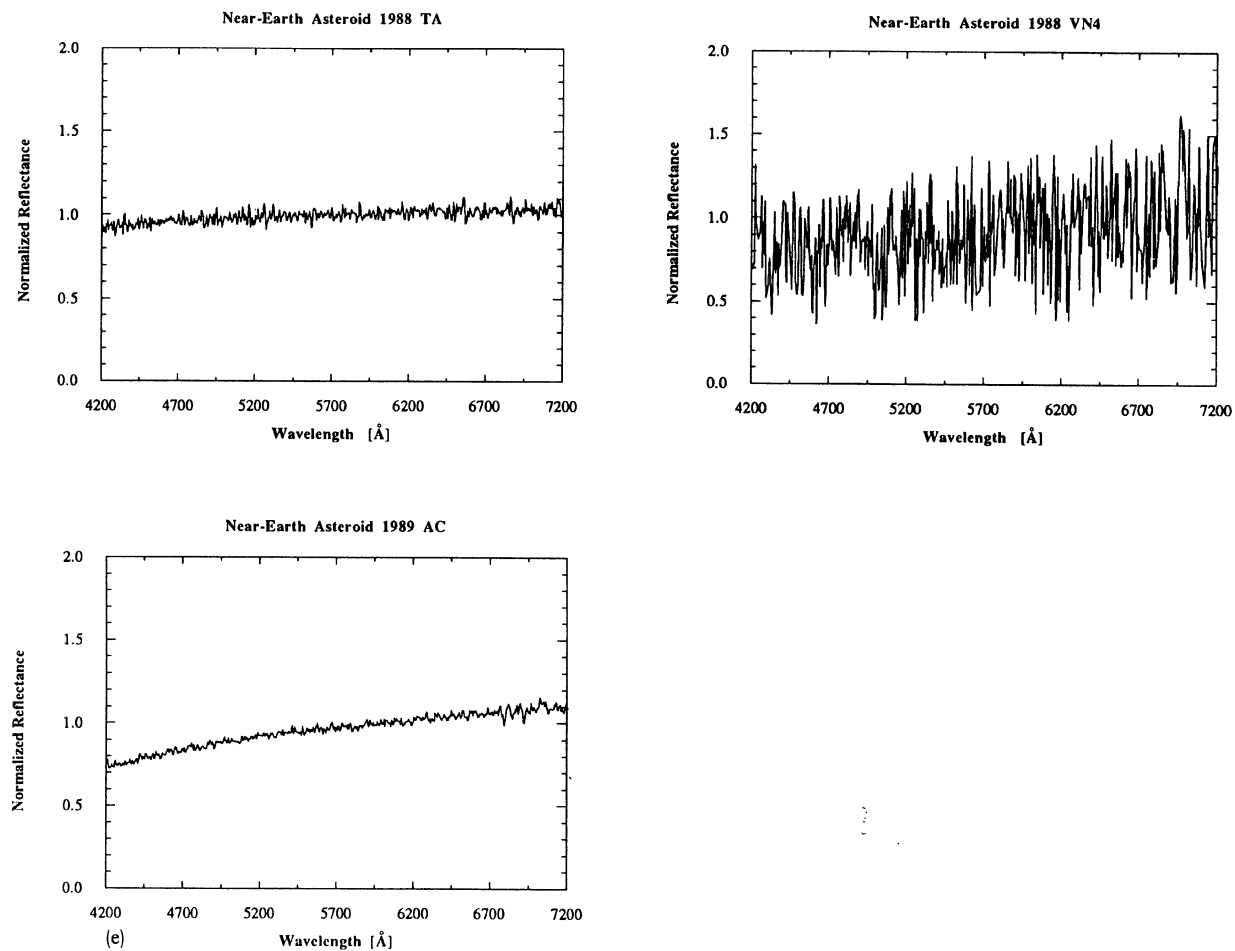


FIG. 4. (continued)

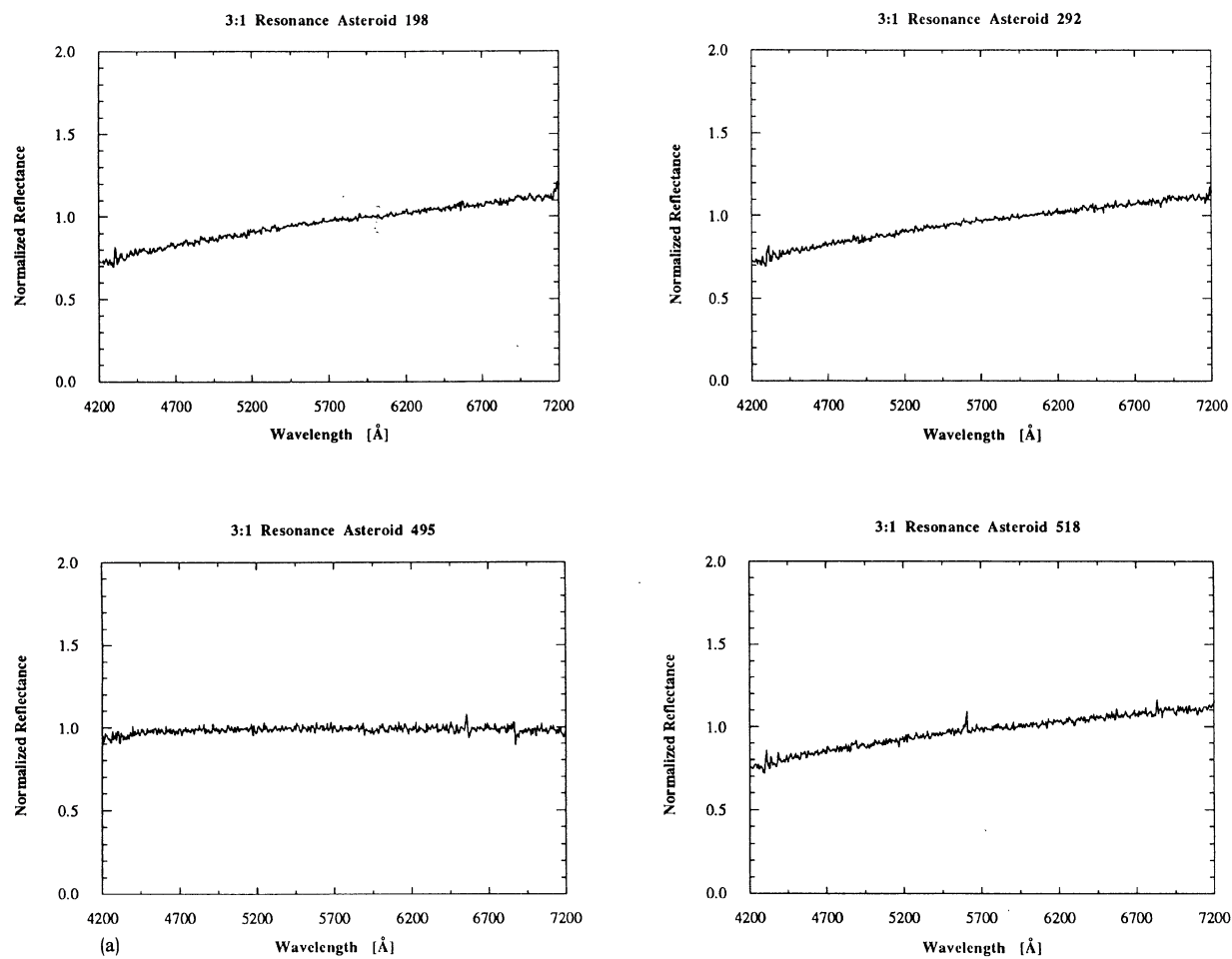


FIG 5. Normalized reflectivity spectra of asteroids near the 3:1 resonance. Features at $\lambda = 5577 \text{ \AA}$, $\lambda = 6300 \text{ \AA}$, $\lambda = 6563 \text{ \AA}$, and $\lambda = 6870 \text{ \AA}$ are due to imperfect removal of sky and solar lines and are not intrinsic to the asteroids.

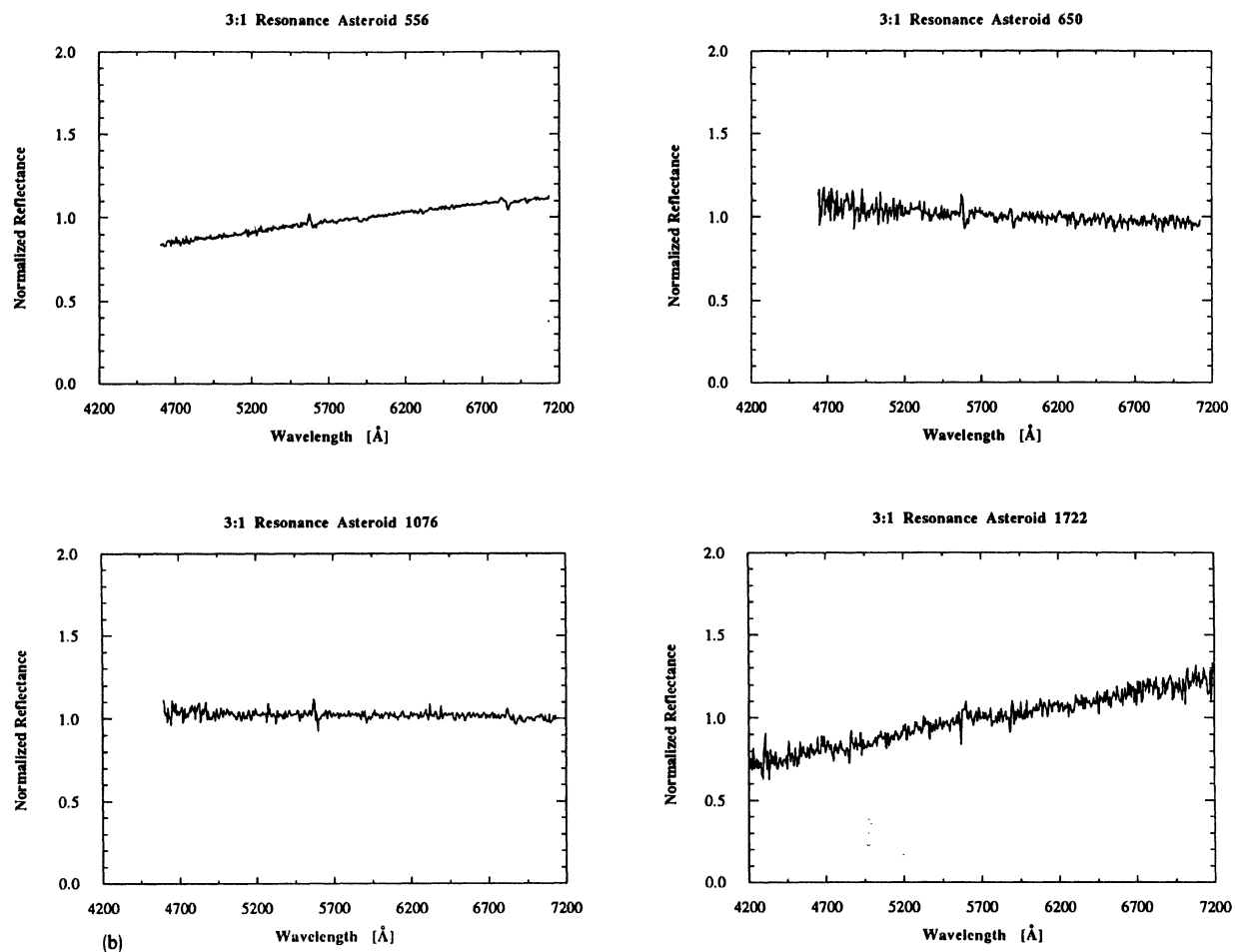


FIG. 5. (continued)

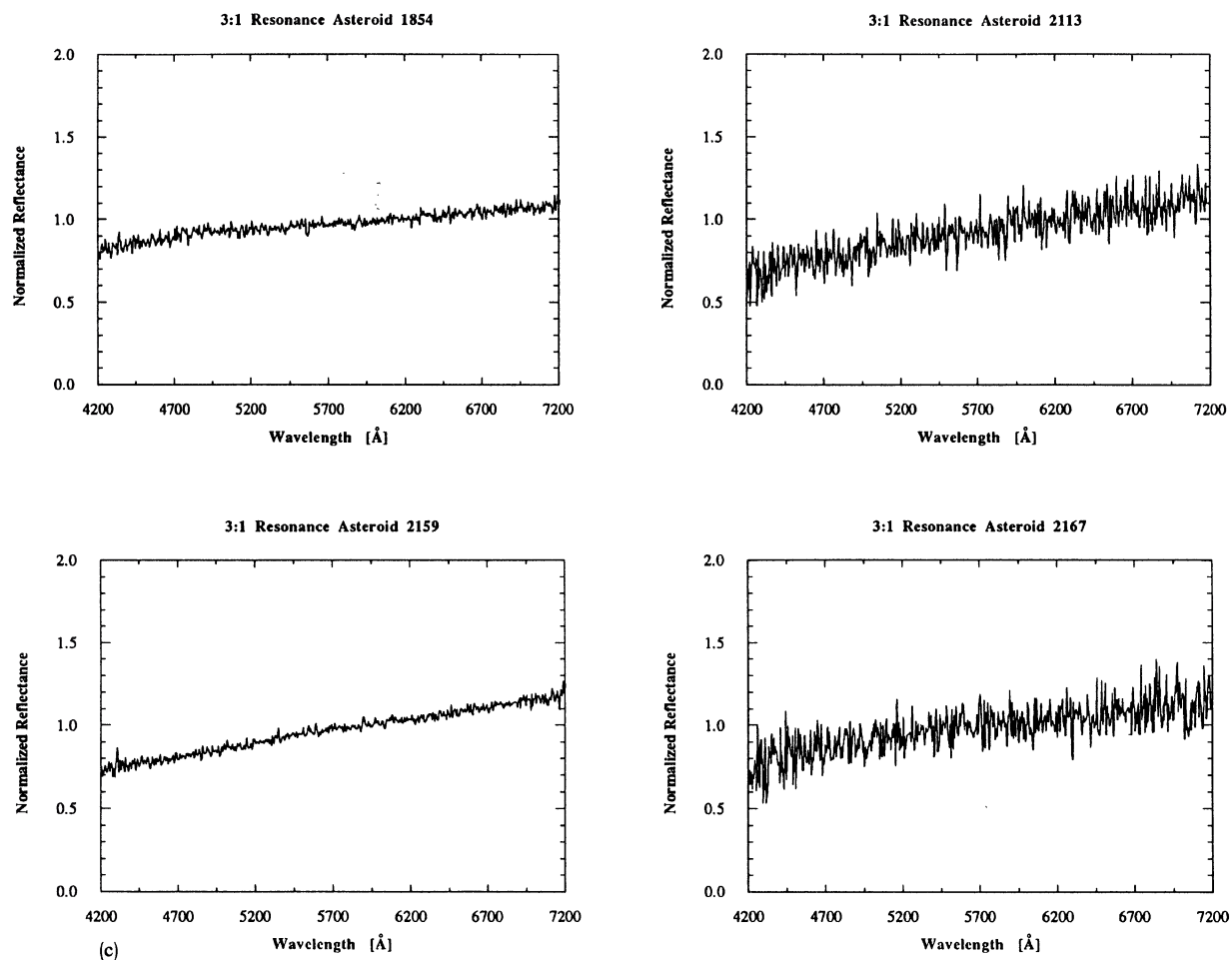


FIG. 5. (continued)

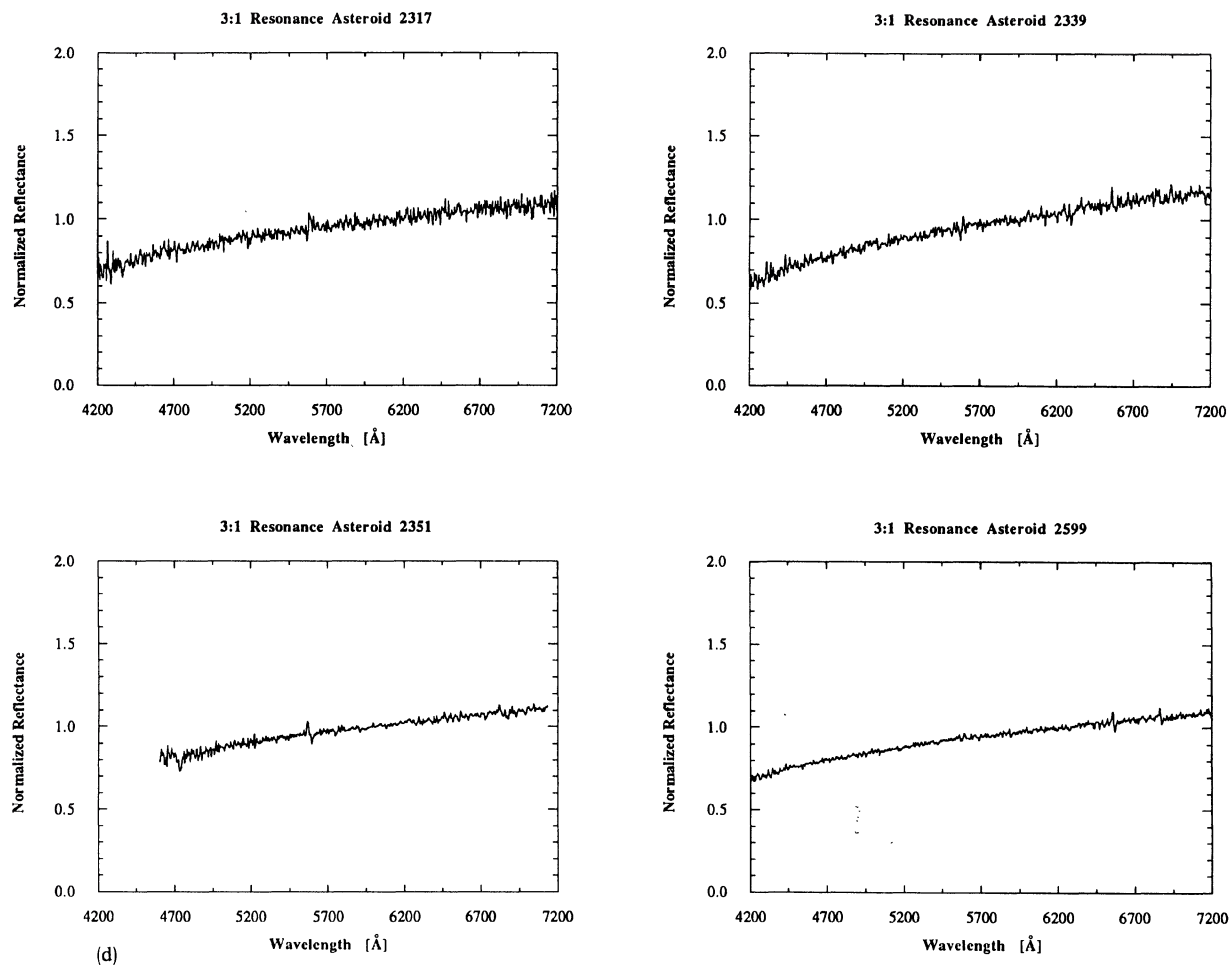


FIG. 5. (continued)

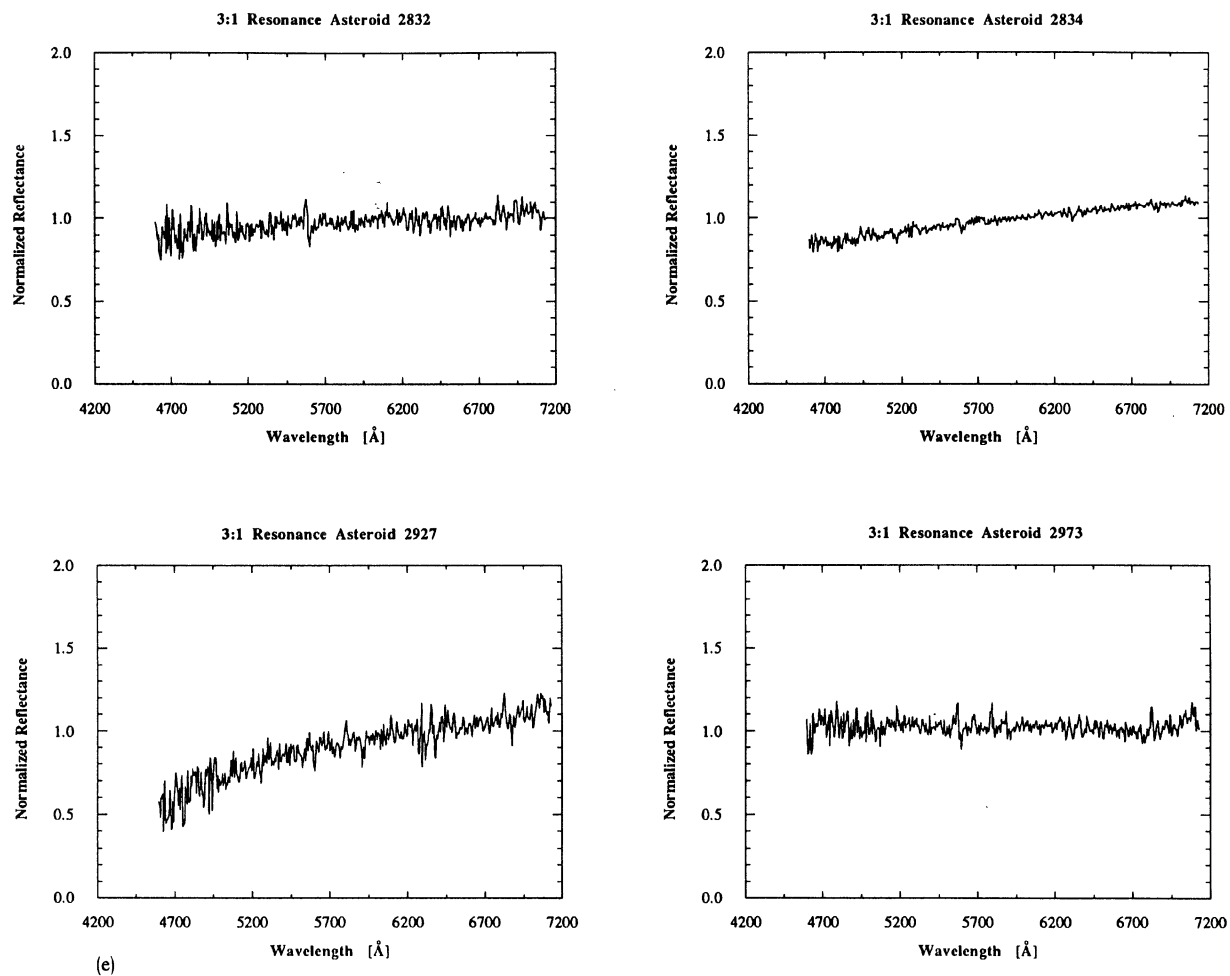


FIG. 5. (continued)

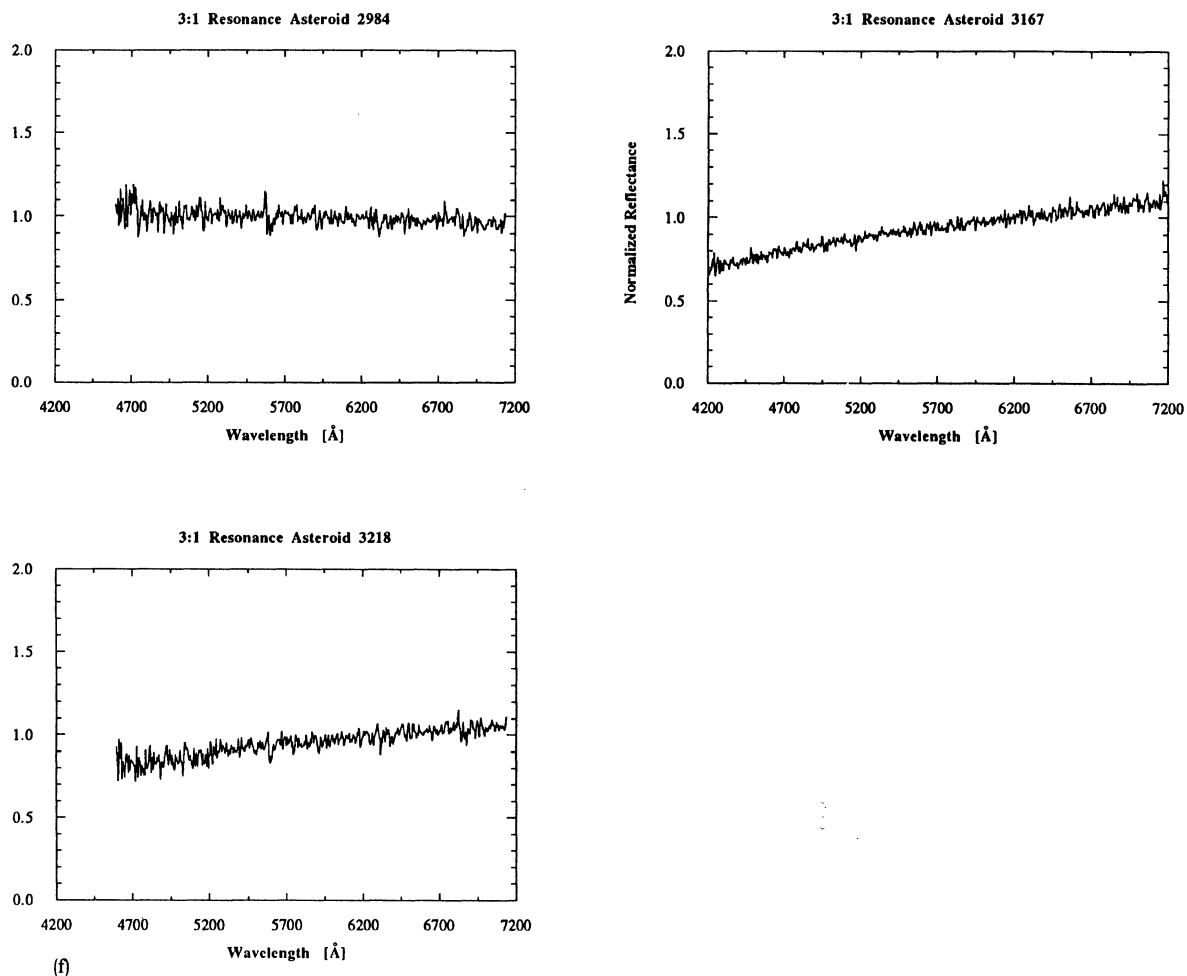


FIG. 5. (continued)

TABLE IV. Near-Earth asteroid reflectivity gradients.

Asteroid	UT Date [Yr Mo Day]	Instrument	Phase [deg]	S' ¹ [%/10 ³ Å]	S'_{true} ² [%/10 ³ Å]
1980	1988 08 08	Mk III	50.5	14.9	6.9
2100	1988 08 08	Mk III	58.1	0.4	-7.6
2212	1988 10 06	GoldCam	10.5	7.1	5.0
3040	1989 02 03	GoldCam	16.6	12.6	9.3
3199	1988 08 05	Mk III	45.5	7.1	-0.9
	1988 10 08	GoldCam	61.3	9.6	1.6
	1988 10 09	GoldCam	61.4	9.4	1.4
3200	1988 10 06	GoldCam	21.8	-8.9	-13.3
3271	1988 08 08	Mk III	48.8	13.0	5.0
3288	1988 08 07	Mk III	11.8	13.6	11.2
3362	1988 08 07	Mk III	63.4	7.7	-0.3
3553	1988 10 08	GoldCam	22.1	14.3	9.9
3691	1989 02 03	GoldCam	18.2	5.3	1.7
	1989 02 08	GoldCam	16.0	5.7	2.5
3752	1988 08 08	Mk III	32.3	14.7	8.3
3838	1988 10 09	GoldCam	48.0	8.5	0.5
	1988 10 08	GoldCam	48.6	10.8	2.8
3908 (1980 PA)	1988 08 07	Mk III	13.1	8.2	5.6
	1988 10 06	GoldCam	34.1	10.2	3.4
	1988 10 10	GoldCam	37.3	11.8	4.3
1987 MB	1988 10 07	GoldCam	7.2	9.6	8.2
1985 DO2 (1988 OG)	1988 09 09	Mk III	14.1	12.7	9.9
1988 TA	1988 10 08	GoldCam	8.8	1.7	-0.1
1988 VN4	1989 02 04	GoldCam	52.6	9.1	1.1
1989 AC	1989 02 04	GoldCam	27.6	9.8	4.3

¹ Apparent S' , uncorrected for phase.² Phase-corrected with the reddening coefficients $\gamma = 0.2$ %/10³ Å/deg ($0^\circ < \alpha \leq 40^\circ$),
 $\gamma = 0$ %/10³ Å/deg ($40^\circ < \alpha$).

TABLE V. 3:1 resonance asteroid reflectivity gradients.

Asteroid	UT Date [Yr Mo Day]	Instrument	Phase [deg]	S^{-1} [%/10 ³ Å]	S'_{true}^2 [%/10 ³ Å]	Asteroid	UT Date [Yr Mo Day]	Instrument	Phase [deg]	S^{-1} [%/10 ³ Å]	S'_{true}^2 [%/10 ³ Å]
198	1988 10 06	GoldCam	26.7	10.6	5.2	2599	1988 09 08	Mk III	02.9	9.8	9.2
292	1988 09 08	Mk III	20.6	11.7	7.6		1988 10 09	GoldCam	14.0	10.5	7.7
	1988 10 06	GoldCam	11.9	10.6	8.2	2832	1988 09 08	Mk III	09.3	3.6	1.7
495	1988 09 08	Mk III	03.7	-2.6	-3.4	2834	1988 09 09	Mk III	06.3	8.9	7.6
	1988 10 10	GoldCam	13.0	-1.4	-4.0	2927	1988 09 08	Mk III	25.1	18.6	13.5
518	1988 09 09	Mk III	25.2	8.6	3.5	2973	1988 09 08	Mk III	07.6	-1.2	-2.7
	1988 10 07	GoldCam	19.0	9.0	5.3	2984	1988 09 09	Mk III	01.9	-3.2	-3.6
556	1988 09 08	Mk III	13.2	10.7	8.1	3167	1988 10 07	GoldCam	19.2	11.0	7.2
	1988 09 09	Mk III	13.5	9.9	7.2		1988 10 08	GoldCam	19.1	11.2	7.4
650	1988 09 09	Mk III	29.3	-5.0	-10.8	3218	1988 09 09	Mk III	03.2	8.7	8.1
1076	1988 09 09	Mk III	03.3	-2.2	-2.8						
1722	1988 10 06	GoldCam	15.4	15.4	12.3						
1854	1988 09 08	Mk III	14.5	10.7	7.8						
	1988 10 06	GoldCam	02.5	6.2	5.7						
2113	1988 10 09	GoldCam	24.2	13.8	9.0						
2159	1988 09 08	Mk III	23.1	14.6	10.0						
	1988 10 06	GoldCam	17.7	13.4	9.9						
2167	1988 09 08	Mk III	8.7	10.6	8.9						
	1988 10 08	GoldCam	16.4	8.8	5.5						
2317	1988 09 08	Mk III	07.0	9.2	7.8						
	1988 10 10	GoldCam	10.5	10.6	8.5						
2339	1988 09 08	Mk III	11.3	10.9	8.6						
	1988 10 09	GoldCam	13.9	11.3	8.5						
2351	1988 09 09	Mk III	03.9	10.7	9.9						

1. Apparent S' , uncorrected for phase.2. Phase-corrected with the reddening coefficients $\gamma = 0.2 \text{ \%}/10^3 \text{ Å}/\text{deg}$ ($0^\circ \leq \alpha \leq 40^\circ$),
 $\gamma = 0 \text{ \%}/10^3 \text{ Å}/\text{deg}$ ($40^\circ < \alpha$).

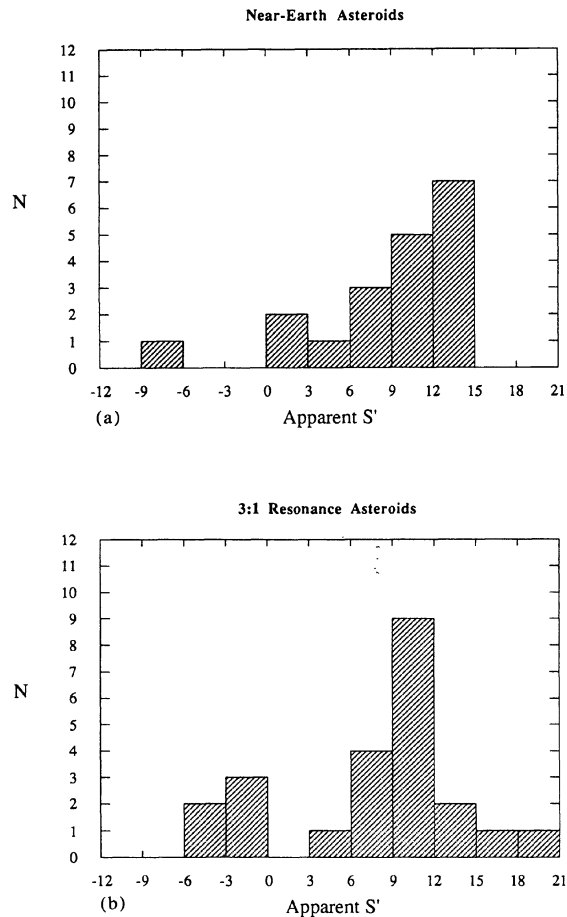


FIG. 6. (a) Histograms of the apparent reflectivity gradient S' (without phase correction) for NEAs and (b) for asteroids near the 3:1 resonance.

histogram [Fig. 6(a)] has a strongly asymmetric shape, with the number of asteroids increasing as S' increases and peaking at $S' = 12\% - 15\% / 10^3 \text{ \AA}$. The resonance asteroid histogram [Fig. 6(b)] is more symmetric, with a peak at $S' = 9\% - 12\% / 10^3 \text{ \AA}$. Our objective is to formally compare the color histograms of the NEAs and resonance asteroids, to see if they are compatible with derivation from a single population. However, before we can make a formal comparison between Figs. 6(a) and 6(b), we must correct for two effects which can distort the shapes of the color histograms, namely, “phase reddening” and “albedo bias.”

V. PHASE-REDDENING CORRECTION

a) The Phase-Reddening Problem

It is known that main-belt asteroids appear redder at large angles than at small angles (Millis *et al.* 1976; Bowell and Lumme 1979; Lumme and Bowell 1981), an effect known as “phase reddening.” This effect has also been observed in the Moon (Gehrels *et al.* 1964; Lane and Irvine 1973), Mars (Irvine *et al.* 1968), and in laboratory experiments with powdered meteorites (Gradie and Veverka 1986). The reddening is due to complex multiple scattering of light in rough surfaces. It is clear that one must correct for phase reddening when comparing the spectra of NEAs and main-belt aster-

oids, since the NEAs tend to be observed at larger phase angles than are the main-belt asteroids (as may be seen from a comparison of Tables II and III). The asymmetric, almost triangular shape of the NEA S' histogram [Fig. 6(a)] directly suggests that S' is affected by phase reddening. Unfortunately, the reddening coefficients vary from material to material, and the reddening coefficients of the specific asteroids observed in this study are unknown. Thus, we must resort to statistical corrections for phase reddening based on evidence from other asteroids.

We define the reddening coefficient γ as

$$\gamma = \frac{dS'}{d\alpha} = \frac{d^2S}{d\alpha d\lambda}, \quad (3)$$

where α is the phase angle. Published reddening coefficients for asteroids can be found in Lumme and Bowell (1981), where the tabulated coefficient (in $m_B - m_V$) for S' types is $\gamma = 0.13\% \pm 0.13\% / 10^3 \text{ \AA/deg}$ and the coefficient for C types is $\gamma = 0.15\% \pm 0.17\% / 10^3 \text{ \AA/deg}$. We know of no published reddening coefficients for asteroids in the color $m_V - m_R$, which more nearly corresponds to the wavelength range of our spectra.

In the present study, a few of the asteroids were observed at more than one phase angle, hence allowing the reddening coefficients to be estimated. Specifically, asteroid 1980 PA (3908) was observed at phase angles $\alpha = 13.1^\circ, 34.2^\circ,$ and 37.3° , giving a best-fit reddening coefficient $\gamma = 0.13\% \pm 0.05\% / 10^3 \text{ \AA/deg}$, while 3199 Nefertiti was observed at $\alpha = 45.5^\circ, 61.3^\circ, 61.4^\circ$, yielding a reddening coefficient $\gamma = 0.15\% \pm 0.01\% / 10^3 \text{ \AA/deg}$. We caution that these coefficients provide only an *estimate* for the magnitudes of the phase reddening effect, since they were derived from a limited phase range. However, the two values measured here are consistent with the means quoted by Lumme and Bowell.

b) The Reddening Correction

Ideally, to correct for phase reddening, we need reddening coefficients for each of the observed asteroids, but these are clearly not available. Instead, we bracket the effects of phase reddening by using the following two correction schemes.

Case (1). We adopt the fitted coefficients

$$\begin{aligned} \gamma &= 0.2\% / 10^3 \text{ \AA/deg} & 0^\circ < \alpha < 40^\circ, \\ \gamma &= 0\% / 10^3 \text{ \AA/deg} & \alpha > 40^\circ. \end{aligned}$$

Case (1) represents the phase reddening suggested by the present asteroid data. Figure 7 shows all our measurements of S' (including those from repeat observations) as a function of phase angle. The empirical data in the figure are represented by two linear fits:

$$\begin{aligned} \gamma &= 0.18\% \pm 0.09\% / 10^3 \text{ \AA/deg}, & 0^\circ < \alpha < 40^\circ, & (4) \\ \gamma &= -0.18\% \pm 0.19\% / 10^3 \text{ \AA/deg}, & 40^\circ < \alpha < 80^\circ. & (5) \end{aligned}$$

The division into two phase angle ranges is suggested by observations of the Moon (one of the few solar system objects that have been studied over a wide range of phase angles), in which the colors of the lunar disk increase linearly with phase in the range $6^\circ \leq \alpha \leq 40^\circ$, and are nearly independent of phase for $40^\circ < \alpha \leq 80^\circ$ (Lane and Irvine 1973). Case (1) does *not* imply that the listed coefficients are the same for all asteroids; it simply allows us to crudely assess the magnitude of the phase-reddening effect on the NEA and resonance colors.

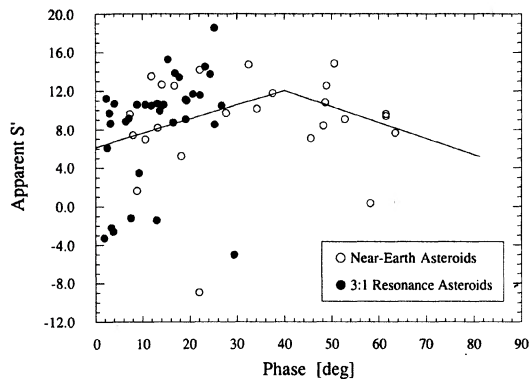


FIG. 7. Plot of apparent S' vs phase for all observed asteroids (repeated observations included). The two straight lines in the phase ranges $0^\circ < \alpha < 40^\circ$ and $40^\circ < \alpha < 80^\circ$ are least-squares fits to the asteroidal S' .

Case (2). We neglect the phase reddening

$$\gamma = 0\%/10^3 \text{ \AA}/\text{deg} \quad (\text{all } \alpha).$$

Clearly, neither case (1) nor case (2) is likely to provide an accurate description of the phase reddening of the asteroids. However, by comparing results obtained using these two extreme cases, we will show below that the general outcome of our comparison does not depend strongly on the method of phase correction.

In Figs. 8(a) and 8(b), we present the histograms of the dereddened S' , which we call S'_{true} [corresponding to case (1)]

$$S'_{\text{true}} = S' - \gamma\alpha. \quad (6)$$

Values of S'_{true} are listed in Tables IV and V. The phase correction removes the triangular asymmetry in the NEA S' distribution [compare Figs. 8(a) and 6(a)], so that the distribution no longer appears to be dominated by reddish asteroids. The histograms corresponding to case (2) are just the apparent S' histograms in Figs. 6(a) and 6(b), which do not include phase correction. The resonance asteroid S' distribution is not much affected by the phase correction, since the range of phase angles is small [Figs. 8(b) and 6(b)].

VI. ALBEDO BIAS CORRECTION

The second correction to be added is the albedo bias correction, probably the most important factor in a statistical comparison of NEAs with other asteroid groups. Both populations of resonance asteroids and NEAs suffer from an observational selection bias toward higher albedo objects. However, due to the different geometries under which the two populations are observed, NEAs and main-belt asteroids exhibit albedo biases of different magnitudes (LJ89). It should be emphasized that, for the purpose of comparing these two populations, only the *difference* in the bias for the two populations matters. (If both populations were observed under the same geometry, there would be no need to apply a bias correction.)

We do not possess albedo determinations for a majority of the observed asteroids. In order to apply the bias correction to the S' distributions, we employed the results of Tholen (1984) and Barucci *et al.* (1987) to establish the relationship between our values of S' and the albedo. From their

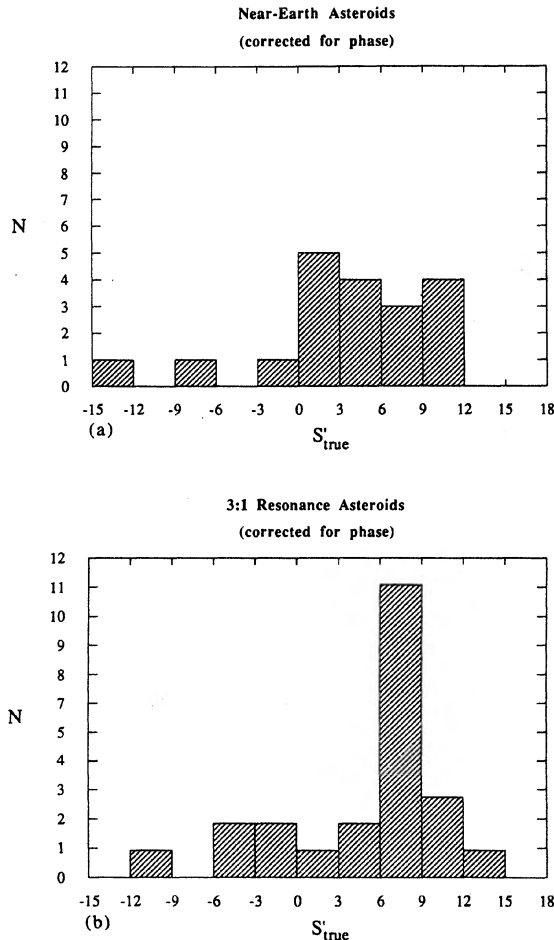


FIG. 8. (a) Histograms of (color-phase corrected) S'_{true} for NEAs and (b) for asteroids near the 3:1 resonance. The phase correction was performed assuming reddening coefficients $\gamma = 0.2\%/10^3 \text{ \AA}/\text{deg}$ ($0^\circ < \alpha < 40^\circ$), $\gamma = 0\%/10^3 \text{ \AA}/\text{deg}$ ($40^\circ < \alpha$) (see Sec. Vb).

classification schemes, we note that a moderate/high albedo (S' type) is generally associated with reddish colors (positive slope in spectrum), with S' in the range $5.0 \leq S' \leq 17.0\%/10^3 \text{ \AA}$ (Tholen 1984). In contrast, a low albedo (C type) is generally associated with neutral or blue colors (flat to negative slope in spectrum), with S' in the range $-4.0 \leq S' < 5.0\%/10^3 \text{ \AA}$ (Tholen 1984). IRAS albedos are available for ten of the observed asteroids (Matson 1986); of these ten, nine obey the S' -albedo relationship described above. Since $\sim 75\%$ of the classified main belt asteroids and NEAs belong to the S or C types (Barucci *et al.* 1987; McFadden *et al.* 1989), we will hereafter broadly classify red asteroids ($5.0 \leq S' \leq 17.0\%/10^3 \text{ \AA}$) as S' types and neutral/blue asteroids ($-4.0 \leq S' < 5.0\%/10^3 \text{ \AA}$) as C types.

[One exception to the S' -albedo relationship is the taxonomic class D, which combines low albedo with a red color. Class D asteroids are believed to be most common in the outer belt and among the Trojans (Gradie and Tedesco 1982), and to date, only two NEAs, 3552 (1983 SA) and 1984 BC, have been classified as class D (Hartmann *et al.* 1987; McFadden *et al.* 1989). In this work, we assume that

class D objects do not contribute significantly to the NEA population.]

The bias correction was carried out using the bias factors of LJ89, which were calculated specifically for *S*- and *C*-type asteroids, assuming a power law size index q in the range $2.0 \leq q \leq 4.0$ (see LJ89 for the bias factors). Typical histograms of the bias-corrected S'_{true} distributions [case (1)] are illustrated in Fig. 9. The histograms in the figure were corrected for the albedo bias assuming $q = 3.0$. With the bias correction included, the NEA distribution [Fig. 9(a)] no longer shows any preponderance of reddish *S*-type asteroids. Rather, it seems to be more dominated by neutral *C* types, peaking near $S'_{\text{true}} \sim 3\%/10^3 \text{ \AA}$ and falling off gradually on both sides of the peak. The bias correction renders the resonance distribution [Fig. 9(b)] more evenly divided over the range $-11 \leq S'_{\text{true}} \leq 14\%/10^3 \text{ \AA}$.

The case (2) counterpart of Fig. 9 is Fig. 10, where we present typical histograms of the apparent S' distributions after the albedo bias correction. It is clear that the lack of phase correction is responsible for the ragged appearance and asymmetry in Fig. 10(a) [compare Figs. 9(a) and

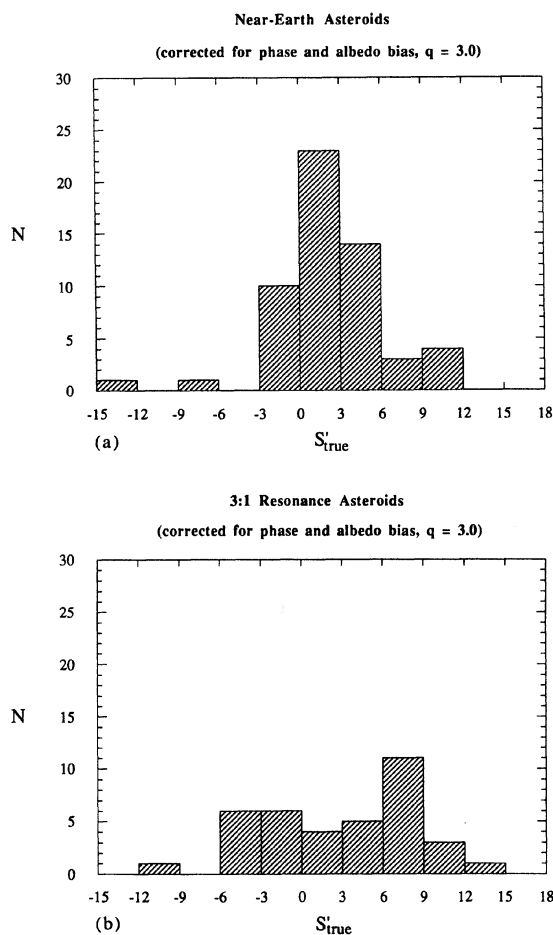


FIG. 9. (a) Case (1) of the analysis: histograms of bias-corrected and color-phase corrected S'_{true} for NEAs and (b) for asteroids near the 3:1 resonance, using power law index $q = 3.0$. The phase correction was performed assuming reddening coefficients $\gamma = 0.2\%/10^3 \text{ \AA}/\text{deg}$ ($0^\circ < \alpha < 40^\circ$), $\gamma = 0\%/10^3 \text{ \AA}/\text{deg}$ ($40^\circ < \alpha$), and the bias correction was performed using bias factors from LJ89.

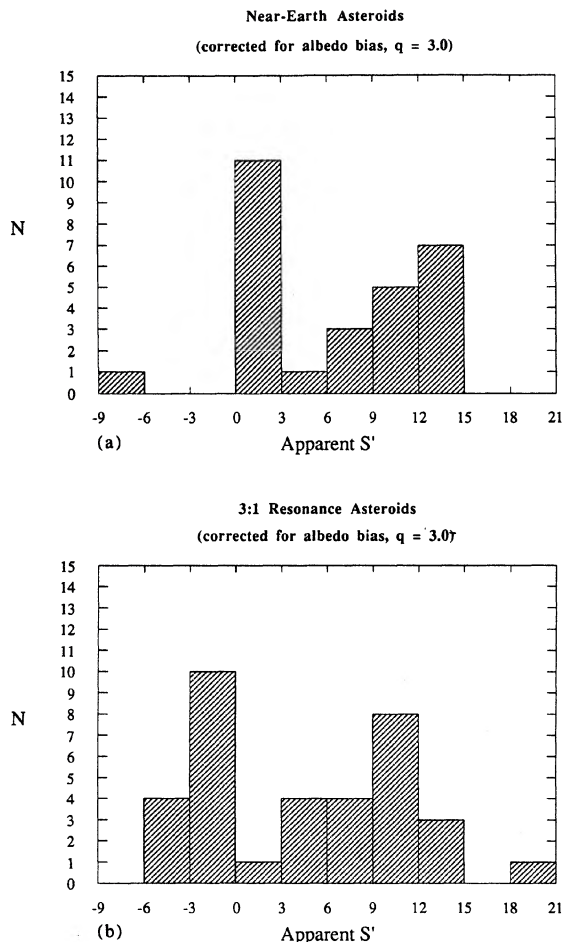


FIG. 10. (a) Case (2) of the analysis: histograms of bias-corrected (but not color-phase corrected) apparent S' for NEAs and (b) for asteroids near the 3:1 resonance, using power law index $q = 3.0$. The bias correction was performed using bias factors from LJ89.

10(a)], yielding the sharp peak (at $S' \sim 2\%/10^3 \text{ \AA}$) superimposed on the asymmetric histogram. As expected, the difference between Figs. 9(b) and 10(b) is less pronounced, since the phase correction does not have a strong effect on the resonance S' distribution.

VII. RESULTS

Visual inspections of Figs. 9(a) and 9(b) and Figs. 10(a) and 10(b) suggest that the NEA and main-belt asteroid color histograms have similar means but have possibly different shapes. However, within the statistical uncertainties, it is not obvious to the eye that the apparent histogram shape difference is significant. For this reason, we resort to nonparametric statistical tests to obtain a formal measure of the degree of similarity between the color histograms.

We apply two statistical tests, the Kolmogorov–Smirnov test and the Mann–Whitney U test, to the S' distributions to test the hypothesis that the two asteroid samples are derived from the same population. Both tests are suitable for the present comparison because they make no assumption on the distribution of the samples to be tested, and because they can be applied easily. The Kolmogorov–Smirnov test is sen-

sitive to all types of differences between two sample distributions, whereas the Mann–Whitney U test is particularly sensitive to a difference in the means of two distributions (e.g., Gibbons 1985).

We test the hypothesis that the two asteroid samples are derived from the same population. The significance criterion is set at the 3σ (0.27%) level. This means that the hypothesis is rejected only when there is less than one chance in 370 that both sample distributions are derived from the same population.

Case (1): We apply the statistical tests to the bias-corrected and color-phase corrected S'_{true} distributions with indices falling in the range $2.0 \leq q \leq 4.0$. We obtain the following results:

Mann–Whitney U test: for all values of q , the hypothesis cannot be rejected.

Kolmogorov–Smirnov test: for all values of q except $q = 4.0$, the hypothesis cannot be rejected. In other words, the color distributions of the NEAs and resonance asteroids are not statistically different (except for the $q = 4$ case). Therefore, our observations are statistically compatible with the hypothesis that the NEAs are derived from the 3:1 resonance, unless $q \geq 4$. However, our observations do not exclude other sources for the NEAs.

Case (2): We apply the statistical tests to the bias-corrected (but not color-phase corrected) apparent S' distributions with indices in the range $2.0 \leq q \leq 4.0$. We obtain the following results:

Mann–Whitney U test: for all values of q , the hypothesis cannot be rejected.

Kolmogorov–Smirnov test: for all values of q except $q = 4.0$, the hypothesis cannot be rejected.

The results from the statistical tests concerning the NEA and resonance asteroid color distributions can be summarized as follows: the distributions are consistent with derivation from a single parent population, unless the size distribution index of the asteroids is very steep ($q \geq 4$). The latter caveat occurs because the albedo bias is a function of q (LJ89). Therefore, in the absence of a direct determination of the size distribution index for the NEAs, there is no basis on which to claim that the color histograms are significantly different from one another. This result reemphasizes the importance of the albedo bias correction to all comparative studies of NEA and main-belt asteroids. The preceding analysis is summarized schematically in Fig. 11.

VIII. DISCUSSION

a) NEA Compositional Distribution

In light of the results from statistical tests, it may be a useful exercise to compare the phase and bias-corrected NEA and resonance distributions in terms of the ratio of the number of S types to the number of C types, Ψ . Our criterion for classifying S and C types was described in Sec. VI. Table VI presents a compilation of Ψ for both the NEA and resonance populations as a function of q . The quoted errors are calculated from Poisson statistics. If we adopt the power law index $q = 3.0$ (as in Figs. 9 and 10), the bias-corrected Ψ ratios are

for the NEAs

$$\Psi_{\text{NEA}} = \begin{cases} 0.2 \pm 0.1:1 & \text{case (1)} \\ 1.4 \pm 1.0:1 & \text{case (2)} \end{cases}, \quad (7)$$

and for the 3:1 resonance asteroids

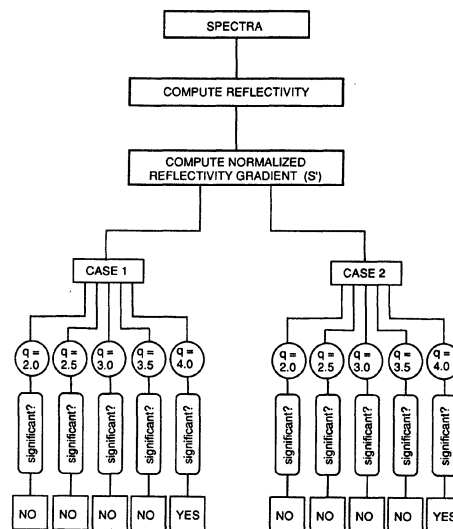


FIG. 11. Flow chart depicting the essential steps of the analysis as described in Secs. IV–VII. The significance level of the difference between the NEA and resonance distributions is determined by the Kolmogorov–Smirnov test. The difference is deemed significant if there is less than a 0.27% (3σ) chance that both sample distributions come from the same population.

$$\Psi_{\text{res}} = \begin{cases} 0.8 \pm 0.4:1 & \text{case (1)} \\ 0.9 \pm 0.5:1 & \text{case (2)} \end{cases}. \quad (8)$$

The importance of the phase reddening correction to the Ψ ratios can be ascertained from the difference between the two values of Ψ_{NEA} [Eq. (7)]. The difference between Eqs. (7) and (8) is consistent with zero at the 3σ level, i.e., the two distributions do not formally differ from one another. Thus our calculated Ψ ratios for the NEAs and resonance asteroids echo the consistency result reached by the statistical tests.

In Table VII, we list Ψ as reported by available optical surveys and the *IRAS* survey, along with the results of this work. We corrected the ratios from the listed optical surveys for the albedo bias where possible; it was not possible to include the phase correction because of lack of sufficient data. The errors listed here are also calculated from Poisson statistics.

It is reassuring to note that Ψ_{res} from the present survey [Eq. (8)] is consistent with previous estimates of Ψ (Table VII). There exists no other bias- and phase-corrected NEA ratio to compare with Ψ_{NEA} from the present survey [Eq. (7)]. However, the compatibility of Ψ_{res} with previously observed ratios implies that, in spite of the lack of albedos and reddening coefficients for each asteroid, the methods adopted to correct for the phase reddening and albedo bias are basically sound. We recognize the fact that the lack of reddening coefficients renders Ψ_{NEA} less certain than Ψ_{res} , since many of the NEAs are observed at much larger phase angles than are the resonance asteroids. This situation is partially remedied by performing the comparison with and without the phase correction [case (1) and case (2)]. Hence the true NEA ratio in our sample lies in the range bounded by the two extreme cases:

TABLE VI. Ratios of S-type to C-type asteroids (ψ) (this work).

Power law index q	NEA			3:1 Resonance		
	observed ψ^2	phase corrected ψ^2	phase and bias corrected ψ^1	observed ψ^2	phase corrected ψ^2	phase and bias corrected ψ^1
2.0	16 : 2	9 : 8	$0.2 \pm 0.1 : 1$	16 : 5	16 : 6	$1.2 \pm 0.6 : 1$
2.5	16 : 2	9 : 8	$0.2 \pm 0.1 : 1$	16 : 5	16 : 6	$1.0 \pm 0.5 : 1$
3.0	16 : 2	9 : 8	$0.2 \pm 0.1 : 1$	16 : 5	16 : 6	$0.8 \pm 0.4 : 1$
3.5	16 : 2	9 : 8	$0.2 \pm 0.1 : 1$	16 : 5	16 : 6	$0.6 \pm 0.3 : 1$
4.0	16 : 2	9 : 8	$0.2 \pm 0.1 : 1$	16 : 5	16 : 6	$0.5 \pm 0.2 : 1$

¹ The bias correction was performed with bias factors from LJ89.

² The listed ratios are the ratios of the numbers of asteroids classified as S-types to the numbers of asteroids classified as C-types (according to the criterion described in §6). Asteroids that do not satisfy the criterion are not included in the ratios.

TABLE VII. Ratios of S-type to C-type asteroids (ψ) (comparison with other works).

Source	NEA			3:1 Resonance		
	observed ψ	phase corr. ψ	bias corr. ψ	observed ψ	phase corr. ψ	bias corr. ψ
Tedesco and Gradie (1987)	24 : 5	---	$0.8 \pm 0.4 : 1^1$	---	---	---
Veeder <i>et al.</i> (1989)	15 : 3	---	$0.9 \pm 0.5 : 1^1$	---	---	---
TRIAD (Zellner 1979)	---	---	---	---	---	0.6 : 1
Gradie and Tedesco (1982)	---	---	---	---	---	0.7 : 1
Gradie <i>et al.</i> (1989)	---	---	---	---	---	0.7 : 1
ECAS (Tholen 1984, Zellner <i>et al.</i> 1985)	11 : 1	---	$1.9 \pm 1.9 : 1^1$	1.9 : 1	---	$0.6 : 1^1$
IRAS (Matson 1986)	---	---	---	0.8 : 1	---	0.8 : 1
This work	16 : 2	9 : 8	$0.2 \pm 0.1 : 1^2$	16 : 5	16 : 6	$0.8 \pm 0.4 : 1^2$

¹ The bias correction was carried out by the authors of this paper, using the LJ89 bias factors corresponding to $q = 3.0$.

² This ratio includes both phase and bias correction, unlike the other ratios in this column.

$$0.2 \pm 0.1:1 \leq \Psi_{\text{NEA}} \leq 1.4 \pm 1.0:1. \quad (9)$$

Equation (9) is consistent with the bias-corrected NEA ratios from other sources at the 3σ level (Table VII). However, the broad range of possible Ψ_{NEA} does not allow an unambiguous determination of the dominant taxonomic type in the NEA population. Either *S* or *C* types could dominate. More stringent limits for Ψ_{NEA} can only be obtained when the NEA size distribution and the asteroidal color-phase coefficients are better determined.

b) Spectral Features

Absorption features are detected in three NEAs (3691, 1980 PA, and 1985 DO2) at $\lambda = 4300 \text{ \AA}$, 4800 \AA , 5050 \AA , and 5500 \AA . We verified their existence using the following observations: (1) the features were reproducible on different nights on different spectrographs (hence they could not be caused by instrumental effects); (2) there are no similar features in the atmosphere or in the solar spectrum (thus they could not be due to errors in background subtraction, extinction correction or solar division); (3) they are independent of standard stars (hence they could not be caused by errors in flux calibration). We therefore conclude that the features are real and are intrinsic to the asteroids.

The NEA 3691 shows a broad absorption band centered at $\sim 4800 \text{ \AA}$; the band is approximately 5% deep and 900 \AA wide (Fig. 4). It was not possible to identify a unique mineral responsible for this feature. Weak bands are also detected in the spectra of 1980 PA and 1985 DO2 at 5050 \AA ($\sim 6\%$ deep and $\sim 200 \text{ \AA}$ wide at the base) and 5500 \AA ($\sim 2\%$ deep and $\sim 360 \text{ \AA}$ wide at the base) (Luu and Jewitt 1989b). Both these bands are likely to come from pyroxene, as is the 4300 \AA feature ($\sim 5\%$ deep and $\sim 650 \text{ \AA}$ wide) in 1980 PA (R. Burns, private communication). The 5050 \AA and 5500 \AA absorption bands have been attributed to forbidden spin transitions of Fe^{2+} indicative of specific pyroxenes (Adams 1975), while the 4300 \AA absorption band comes from charge transfer between Fe^{2+} and Fe^{3+} (Burns *et al.* 1972). The 4300 \AA band is presumably present in 1985 DO2 also, but the more limited range of the 1985 DO2 spectrum does not allow detection of the band. All the features mentioned above have been observed in lunar pyroxenes from the Apollo 11, 12, 14, 15 missions (Burns *et al.* 1972) but, to our knowledge, have not been detected in any asteroid. The stronger $0.9 \mu\text{m}$ absorption feature due to pyroxene has also been observed in the spectra of 1980 PA and 1985 DO2, similar to that observed in asteroid 4 Vesta (McCord *et al.* 1970), whose taxonomic class V had included only two asteroids until now (Tholen 1988). For clarity, the spectra of 1980 PA and 1985 DO2 are shown again in Fig. 12, along with the spectrum of Vesta (Luu and Jewitt 1989, unpublished data). We note that no absorption features were detected among the observed resonance asteroids, in spite of the comparably high signal-to-noise ratio in 13 of the resonance asteroid spectra.

IX. SUMMARY

We have attempted a systematic comparison of the visual reflectivities of 19 NEAs and 23 asteroids from near the 3:1 resonance in the main belt. This comparison was undertaken in order to test the hypothesis that the NEAs are derived from the 3:1 resonance. Our work is founded on new, high-quality CCD spectra of the asteroids, taken and reduced according to uniform experimental procedures. We find that the quantitative comparison of the two asteroid groups is a

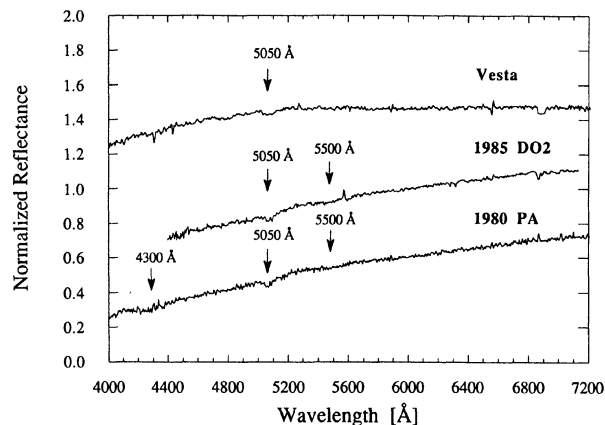


FIG. 12. Reflectivity spectra of main-belt asteroid 4 Vesta, and NEAs 1985 DO2 and 1980 PA. The normalized spectra were arbitrarily shifted in the vertical direction for ease of comparison. Features at $\lambda = 5577 \text{ \AA}$, $\lambda = 6300 \text{ \AA}$, $\lambda = 6563 \text{ \AA}$, and $\lambda = 6870 \text{ \AA}$ are due to imperfect removal of sky and solar lines and are not intrinsic to the asteroids. Intrinsic asteroidal absorption features at $\lambda = 5050 \text{ \AA}$ and $\lambda = 5500 \text{ \AA}$ are marked by arrows.

surprisingly difficult exercise. The difficulties arise from the need to incorporate phase reddening and albedo-bias correction factors. We parameterize the phase-reddening relationship using two limiting cases, while we take the albedo-bias correction factors from a published Monte Carlo simulation (LJ89a).

(1) The phase reddening and (especially) the albedo-bias corrections are sufficiently large that they cannot be ignored if a physically meaningful comparison of the NEA and main-belt asteroid populations is to be obtained.

(2) For power law size indices $2.0 \leq q \leq 3.5$, the hypothesis that the NEAs and the resonance asteroids are drawn from the same population cannot be rejected on the basis of the new data. For $q = 4.0$, the hypothesis can be rejected. Hence, for all but the steepest size distributions, our study is consistent with the notion that the 3:1 resonance region is a major source of the NEAs, as has been suggested from dynamical considerations. However, other possible sources of NEAs are not excluded by the observations.

(3) The same result (consistency between the color distributions of the NEAs and 3:1 resonance asteroids for most plausible size distributions) is reached with or without the phase-reddening correction.

(4) Three out of 19 observed NEAs (3691, 1980 PA, 1985 DO2) exhibit distinct absorption features. Bands at 5050 \AA and 5500 \AA are due to spin-forbidden transitions of Fe^{2+} , probably in pyroxene. A band at 4300 \AA in the spectrum of 1980 PA is attributed to charge transfer (Fe^{2+} to Fe^{3+}) in pyroxene while a broad feature at 4800 \AA in the spectrum of 3691 is unidentified. None of the 13 main-belt asteroids observed at comparably high signal-to-noise ratio show similar features.

We are grateful to R. Binzel and M. Gaffey for their helpful comments, and to the McGraw-Hill and Kitt Peak staff for their help with the instruments. Special thanks go to George Will for expert operation of the 2.1 m telescope during our October 1988 run. This work was supported by a NASA Graduate Student Fellowship to JXL and by a grant to DCJ from the NASA Planetary Astronomy Program.

REFERENCES

- Adams, J. B. (1975). In *Infrared and Raman Spectroscopy of Lunar and Terrestrial Minerals*, edited by C. Karr, Jr. (Academic, New York), pp. 91–116.
- Barucci, M. A., Capria, M. T., Coradini, A., and Fulchignoni, M. (1987). *Icarus* **72**, 304.
- Bowell, E., and Lumme, K. (1979). In *Asteroids*, edited by T. Gehrels (University of Arizona, Tucson), pp. 132–169.
- Burns, R. G., Abu-Eid, R. M., and Huggins, F. E. (1972). In *Proceedings of the Third Lunar Science Conference, Geochimica et Cosmochimica Acta* (MIT, Cambridge), Vol. 1, pp. 533–543.
- Conover, W. J. (1980). *Practical Nonparametric Statistics*, 2nd ed. (Wiley, New York), pp. 216–223.
- Dickinson, J. G. (1985). *Nonparametric Methods for Quantitative Analysis*, 2nd ed. (American Science, Inc., Columbus), pp. 250–258.
- Drummond, J. D. (1982). *Icarus* **49**, 143.
- Ephemerides of Minor Planets* (1988). Institute for Theoretical Astronomy, Leningrad, USSR.
- Filippenko, A. V. (1982). *Publ. Astron. Soc. Pac.* **94**, 715.
- Gehrels, T., Coffeen, T., and Owings, D. (1964). *Astron. J.* **69**, 826.
- Gibbons, J. D. (1985). *Nonparametric Statistical Inference*, 2nd ed. (Marcel Dekker, New York), pp. 122–150.
- Gradie, J., and Tedesco, E. (1982). *Science* **216**, 1405.
- Gradie, J., and Veverka, J. (1986). *Icarus* **66**, 455.
- Gradie, J., Chapman, C., and Tedesco, E. F. (1989). In *Asteroids II*, edited by R. Binzel, T. Gehrels, and M. S. Matthews (University of Arizona, Tucson), pp. 316–335.
- Hahn, G., and Rickman, H. (1985). *Icarus* **61**, 417.
- Hardorp, J. (1978). *Astron. Astrophys.* **63**, 383.
- Hardorp, J. (1980). *Astron. Astrophys.* **91**, 221.
- Hartmann, W. K., Tholen, D. J., and Cruikshank, D. P. (1987). *Icarus* **69**, 33.
- Irvine, W. M., Simon, T., Menzel, D. H., Pikoos, C., and Young, A. T. (1968). *Astron. J.* **73**, 807.
- Lane, A. P., and Irvine, W. M. (1973). *Astron. J.* **78**, 267.
- Lumme, K., and Bowell, E. (1981). *Astron. J.* **86**, 1705.
- Luu, J., and Jewitt, D. (1989a). *Astron. J.* **98**, 1905 (LJ89).
- Luu, J., and Jewitt, D. (1989b). IAU Circular No. 4722.
- Matson, D. (Ed.) (1986). *IRAS Asteroid and Comet Survey: Preprint Version No. 1* (JPL Internal Document No. 3698), Part III.
- McCord, T. B., Adams, J. B., and Johnson, T. V. (1970). *Science* **168**, 1445.
- McCord, T. B., Adams, J. B., Gaffey, M. J., and McCord, T. B. (1984). *Icarus* **59**, 25.
- McCord, T. B., Gaffey, M. J., and McCord, T. B. (1985). *Science* **229**, 160.
- McCord, T. B., Tholen, D. J., and Veeder, G. J. (1989). In *Asteroids II*, edited by R. Binzel, T. Gehrels, and M. S. Matthews (University of Arizona, Tucson), pp. 442–467.
- Mendenhall, W., Scheaffer, R. L., and Wackerly, D. D. (1986). *Mathematical Statistics with Applications*, 3rd ed. (PWS, Boston), pp. 621–629.
- Millis, R. L., Bowell, E., and Thompson, D. T. (1976). *Icarus* **28**, 53.
- Oke, J. B. (1974). *Astrophys. J. Suppl.* **27**, 21.
- Olsson-Steel, D. (1988). *Icarus* **75**, 64.
- Ostro, S. J. (1985). *Publ. Astron. Soc. Pac.* **97**, 877.
- Shoemaker, E. M., Williams, J. G., Helin, E. F., and Wolfe, R. F. (1979). In *Asteroids*, edited by T. Gehrels (University of Arizona, Tucson), pp. 253–282.
- Shoemaker, E. M., and Wolfe, R. F. (1986). In *The Galaxy and the Solar System*, edited by R. Smoluchowski, J. N. Bahcall, and M. S. Matthews (University of Arizona, Tucson), pp. 338–386.
- Stone, R. P. S. (1977). *Astrophys. J.* **218**, 767.
- Tedesco, E. F., and Gradie, J. (1987). *Astron. J.* **93**, 738.
- Tholen, D. J. (1984). Ph. D. dissertation, University of Arizona, Tucson.
- Tholen, D. J. (1988). IAU Circular 4655.
- Veeder, G. J., Hanner, M. S., Matson, D. L., Tedesco, E. F., Lebofsky, L. A., and Tokunaga, A. T. (1989). *Astron. J.* **97**, 1211.
- Wetherill, G. W. (1988). *Icarus* **76**, 1.
- Whipple, F. L. (1983). IAU Circular 3881.
- Wisdom, J. (1982). *Astron. J.* **87**, 577.
- Wisdom, J. (1983). *Icarus* **56**, 51.
- Zellner, B. (1979). In *Asteroids*, edited by T. Gehrels (University of Arizona, Tucson), pp. 783–806.
- Zellner, B., Tholen, D. J., and Tedesco, E. F. (1985). *Icarus* **61**, 355.